# Scheduling distributed energy resources and smart buildings of a Microgrid via multi-time scale and model predictive control method

Xiaolong Jin [1], Tao Jiang [2*], Yunfei Mu [1*], Chao Long [3], Xue Li [2], Hongjie Jia [1], Zening Li [2]

[1] Key Laboratory of Smart Grid of Ministry of Education, Tianjin University, Tianjin 300072, China
[2] Department of Electrical Engineering, Northeast Electric Power University, Jilin, Jilin 132012, China
[3] Institute of Energy, School of Engineering, Cardiff University, Cardiff CF24 3AA, UK
[*] tjiang@neepu.edu.cn, yunfeimu@tju.edu.cn

**Abstract: To schedule the distributed energy resources (DERs) and smart buildings of a Microgrid in an optimal way and consider the uncertainties associated to forecasting data, a two-stage scheduling framework is proposed in this paper. In stage I, a day-ahead dynamic optimal economic scheduling method is proposed to minimise the daily operating cost of the Microgrid. In stage II, a model predictive control based intra-hour adjustment method is proposed to reschedule the DERs and smart buildings to cope with the uncertainties. A virtual energy storage system is modelled and scheduled as a flexible unit using the inertia of building in both stages. The underlying electric network and the associated power flow and system operational constraints of the Microgrid are considered in the proposed scheduling method. Numerical studies demonstrate that the proposed method can reduce the daily operating cost in stage I and smooth the fluctuations of the electric tie-line power of the Microgrid caused by the day-ahead forecasting errors in stage II. Meanwhile, the fluctuations of the electric tie-line power with the MPC based strategy are better smoothed compared with the traditional open-loop and single-period based optimisation methods, which demonstrates better performance of the proposed scheduling method in a time-varying context.**

## NOMENCLATURE

| | |
|---|---|
| ***Abbreviations:*** | |
| HAVC | Heating, ventilation, and air conditioning. |
| VESS | Virtual energy storage system. |
| BIM | Buildings-integrated-Microgrid. |
| DER | Distributed energy resource. |
| DG | Distributed generator. |
| PV | Photovoltaic. |
| BEMS | Energy management system of building. |
| MEMS | Energy management system of Microgrid. |
| MPC | Model predictive control. |
| ***Sets and indices:*** | |
| $J$, $j$ | Set of indexes of the wall orientations of a building. |
| $T$, $t$ | Set of indexes of the scheduling time periods. |
| $DG$, $i$ | Set of indexes of the controllable DGs. |
| $BD$, $m$ | Set of indexes of the buildings. |
| $EC$, $n$ | Set of indexes of the electric chillers. |
| ***Parameters and constants:*** | |
| $C_{ph}$, $C_{se}$ | Electricity purchasing/ selling prices ($/kWh). |
| $P_{el,m}$ | Electric load of building $m$ (kW). |
| $P_{load}$ | Electric load of the Microgrid except the electric load of buildings (kW). |
| $P_{PV}$, $P_{WT}$ | Electric power generated by photovoltaic system and wind system (kW). |
| $U_{wall}$, $U_{win}$ | Heat transfer coefficient of the wall/window of the building [W/(m$^2$·K)]. |
| $F_{wall,j}$ | The area of the total wall surface at the $j^{th}$ wall orientation (m$^2$). |
| $F_{win,j}$ | The area of the total window surface at the $j^{th}$ wall orientation (m$^2$); It is assumed that the total window surfaces are distributed in the south, west, north and east orientations of the walls in a building uniformly. |
| $T_{out}$ | Outdoor temperature (ºC). |
| $\tau_{win}$ | The glass transmission coefficient of the windows. |
| $SC$ | The shading coefficient of the windows. |
| $\alpha_w$ | Absorbance coefficient of the external surface of the wall. |
| $\dot{Q}_{in}$ | Internal heat gains from people, appliances and lighting (kW). |
| $\rho$, $C$, $V$ | The density (kg/m$^3$), specific heat capacity [J/(kg·ºC)] and volume of the air (m$^3$) in the building. |
| $R_{se,j}$ | The external surface heat resistance for convection and radiation of the external wall $j$ (m$^2$·K/W). |
| $I_{T,j}$ | The total solar radiation on the walls/ windows surface at the $j$-wall orientation (kW/m$^2$). |
| $EER_{EC}$ | Energy efficiency ratio of the EC. |
| $\rho$ | Maintenance cost of the energy devices ($/kWh). |
| $\overline{Q}_{EC}$ | The upper limit of the cooling power output of the EC (kW). |
| $\overline{T_{in}}$, $\underline{T_{in}}$ | The upper and lower limits of the indoor temperature set-points of the building (ºC). |
| $\overline{P_{grid}}$, $\underline{P_{grid}}$ | The upper and lower limits of electric power exchange with the utility grid of the building (kW). |
| $\overline{P_{bt}}$, $\underline{P_{bt}}$ | The upper and lower limits of charging/discharging power of the battery (kW). |
| $\overline{P_{DG}}$, $\underline{P_{DG}}$ | The upper and lower limits of power generation of DG (kW). |
| $R_u$, $R_d$ | Ramp-up/ramp-down rate of a controllable DG (kW/min). |
| $S_u$, $S_d$ | Startup/shutdown rate of a controllable DG (kW/min). |
| $UT$, $DT$ | Minimum up/down time periods of a controllable DG (h). |
| $a$, $b$, $c$ | Fuel cost coefficients of the diesel engine. |
| $\eta_{FC}$ | Efficiency of the fuel cell. |
| $\eta_{ch}$, $\eta_{dis}$ | Charging/discharging efficiency of the battery. |
| $CAP_{bt}$ | The rated capacity of the battery (kWh). |

| | |
|---|---|
| $SOC$, $\delta$ | The state of charge/self-discharge ratio of the battery. |
| ***Variables:*** | |
| $P_{grid}$ | Electric power exchange with the utility grid (kW). |
| $P_{gas}$ | Natural gas consumption (kW). |
| $P_{EC}$ | Electric power consumption by the EC (kW). |
| $P_{loss}$ | Power loss of the electric network (kW). |
| $\dot{Q}_{EC}$ | Cooling power generated by the EC (kW). |
| $\dot{Q}_{wall}$ | Heat transfer through the external walls (kW). |
| $\dot{Q}_{win}$ | Heat transfer across the windows (kW). |
| $\dot{Q}_{sw}$ | Heat contribution due to the solar radiation on the opaque surface of the external walls (kW). |
| $\dot{Q}_{sg}$ | The whole solar radiation transmitted across the windows (kW). |
| $\dot{Q}_{cl,building}$ | Cooling load of the Microgrid with VESS being scheduled (kW). |
| $\dot{Q}'_{cl,building}$ | Cooling load of the Microgrid without VESS being scheduled (kW). |
| $P_{bt}$ | Charging/discharging power of battery (kW). |
| $P_{DG}$ | Power generation of DG (kW). |
| $U_{DG}$ | Operation status of DG, where "1" represents 'ON'-state and "0" represents 'OFF'-state. |
| $U'_{DG}$, | Startup status of DG, which is "1" for startup and "0" for otherwise. |
| $U''_{DG}$ | Shutdown status of DG, which is "1" for shutdown and "0" for otherwise. |
| $T^{on}$, $T^{off}$ | Number of successive ON/OFF time periods of DG (h). |
| $T_{in}$ | Indoor temperature (°C). |

## 1. Introduction

### *1.1. Background*

The recent years experienced a rapid increase of power consumption in buildings worldwide due to the rapid process of urbanization of the world's population [1]. It has been shown that global use of electricity in buildings grew on average by 2.5% per year since 2010, and it increased by nearly 6% per year [2]. According to the International Energy Agency, buildings' share of the worldwide energy usage is approximately 40%, with almost half of it being used in their heating, ventilation and air conditioning (HVAC) systems [3]. After more than 30 years of rapid economic development, China has become a large $CO_2$ emitter with its increasing energy consumption [4]. The building sector currently accounts for 27.6% of the total energy use and it is estimated to reach 35% by 2020 in China [5]. Therefore, issues on energy consumption reduction of buildings will become more prominent in China.

### *1.2. Motivation*

Power consumption related to thermal appliance operation for heating/cooling purposes in a building, such as HVAC and electric chiller, represents a very high portion in load demand. For most of the applications of heating/cooling devices, it is only required to control the temperature in a suitable zone without disturbing the temperature comfort level [6]. This provides an opportunity to effectively reduce the energy usage/cost and the peak demand of buildings by scheduling the heating/cooling devices in an optimal way. Hence in principle, buildings have the potential to become a huge source of flexibility to reduce the load demand, facilitate integration of intermittent renewable generation and provide ancillary services to power systems [6].

Microgrids offer an opportunity and a desirable infrastructure to schedule smart buildings of a community in an optimal way by utilizing advanced energy management technologies and intelligent communication technologies [7]. It leads to the concept of Buildings-integrated-Microgrid (BIM). Several benefits and opportunities can be achieved by applying the Microgrid energy management on the BIM system: 1) Buildings can enjoy energy/cost savings [8]; 2) Intermittent renewable generation can be more efficiently integrated [9]; 3) Distributed energy resources (DERs) at building side, such as controllable distributed generators (DG), storage devices and electric vehicles, are more efficiently managed [10]; 4) Power imbalance of the Microgrid can be balanced by optimal scheduling the DER and smart buildings without being charged for reserve service from the utility grid [11]. Therefore, Microgrid energy management in buildings is attracting more and more attentions in recent years. The PV and wind based DGs are uncontrollable due to their characteristics of randomness and intermittent. In this context, the PV and wind based DGs are not included in the investigated DERs in this paper.

### *1.3. Related work and research gaps*

Studies have been carried out to investigate the energy management methods for a BIM. Optimal day-ahead scheduling methods were investigated for a BIM in [9]-[14] achieving different operational objectives, such as operating cost reduction and pollutants emission reduction. The main idea is that optimisation technologies are used to decide day-ahead optimal schedules of the BIM based on day-ahead forecasting data, day-ahead electricity prices and technical information of energy devices of the BIM. However, the inherent uncertainties of the day-ahead forecasting data are not considered, which leads to a discrepancy between the power really exchanged with the utility grid and the planned one. To further consider the uncertainties associated to the day-ahead forecasting data, stochastic day-ahead scheduling methods were proposed in [15] and [16] by using scenario-based method and scenarios reduction techniques. Nevertheless, the stochastic optimal scheduling methods assume the day-ahead forecasting data follows certain probability density functions. The probability density functions require sufficient historical data, which limits the application of the stochastic method [17]. Meanwhile, the probability density functions may be inappropriate to describe the uncertainties in practical applications [18]. Robust day-ahead scheduling method is another way to consider the uncertainties for scheduling a BIM, as proposed in [19][20]. However, concerns of its practical application are the conservativeness, as the robust optimal scheduling method is based on the worst-case analysis [21]. The above optimal day-ahead scheduling methods have made good contributions to the optimisation of a BIM. However, since the operational time scales of a BIM system are different between the day-ahead stage and actual operational stage, the day-ahead methods with one single time scale are difficult to capture the temporal dependencies of the schedules of the DERs and smart buildings between the two stages. In this context, the optimal schedules determined by the day-ahead methods leave questions on their feasibility and actual performances for practical applications on the BIM. Furthermore, although the uncertainties of the day-ahead forecasting data are considered at day-ahead scheduling stage, their dynamic random fluctuations are not considered at

actual operational stage, which still causes errors between the schedules of two stages and further induces fluctuations of the electric tie-line power of the BIM. As stated in [22], balancing the errors and smoothing the fluctuations are important for the benefits of the utility grid and the BIM.

To cope with the above problems, multi-time scale and multi-stage scheduling methods for BIM system have gained much attentions recently. A multi-time scale and coordinated scheduling method for a multi-energy BIM was proposed in [22]. A two-stage robust scheduling method for a BIM system was proposed in [23] to minimize the operating cost. A multi-time scale stochastic scheduling method was proposed in [24] to schedule deferrable appliances and energy resources of a smart building in an optimal way considering the uncertainties of forecasting data. However, the flexibility of the building with heat inertia has not been fully explored in the above work. In [25], a two-stage hierarchical Microgrid energy management method in an office building by scheduling thermal mass of the building and plug-in electric vehicles was proposed. The daily operating cost can be reduced at the day-ahead stage and the fluctuations of the electric tie-line power can be smoothed to some extent at the intra-hour stage with the proposed method. Although the flexibility of the building was considered in [25], the optimal scheduling method used at actual operational stage was open-loop and single-period based in nature. In other words, the optimal schedules at actual operational stage are optimized using the single-period based optimisation strategy based on the operating status of the BIM and forecasting data at current operational period rather than the predictive operating status and forecasting data over a future time horizon [26]. In this case, concerns regarding the optimal adjustments of the controllable units of the BIM at the actual operational stage, such as insufficient adjustments, excessive adjustments and untimely adjustments, would arise [27]. This leads to bad control performance of the single-period optimisation strategy in a time-varying context with uncertainties associated to forecasting data.

Different to the open-loop and single-period strategy, model predictive control (MPC) based scheduling method leads to better control performance against uncertainties because of its capability to handle the future behaviour of the BIM system, demand and renewable generation forecasts and the constraints of the BIM. MPC computes a sequence of decision variable adjustments over a future time horizon iteratively based on an underlying optimisation model and forecasting data of uncertain variables [28]. In other words, MPC is a rolling process that runs the embedded optimisation model repeatedly with updated forecasts, which has better control performance in a time-varying context, as verified in [29]. Motivated by the attractive features of MPC method in time-varying context, an MPC-based scheduling strategy for the BIM is developed at the intra-hour adjustment stage in this paper. The intra-hour adjustment stage can smooth the fluctuations of the electric tie-line power of the BIM caused by the errors of the day-ahead forecasting data.

Furthermore, these existing approaches consider the aggregate supply-demand balance while omitting the underlying electric network, the associated power flow (e.g., Kirchhoffs laws), and system operational constraints (e.g., voltage tolerances). Consequently, such approaches may result in control decisions that violate the real-world constraints [30]. Therefore, this paper focuses on developing an optimal scheduling method for a Microgrid via multi-time scale and model predictive control method. The power flow and system operational constraints of the electric network of the Microgrid is considered in the proposed scheduling method.

### *1.4. Contributions of this paper*

To schedule the DERs and smart buildings of a Microgrid more efficiently and bridge the research gaps, a novel two-stage scheduling method for a BIM system via multi-time scale and MPC method is proposed in this paper. The main contributions are summarized as follows:

1) A novel two-stage method is proposed for scheduling DERs and smart buildings of a Microgrid by using multi-scale and MPC method. The proposed scheduling method consists of a day-ahead dynamic optimal economic scheduling stage and an intra-hour rolling adjustment stage. The framework takes care of two different objectives, i.e., reducing the daily operating cost and smoothing the fluctuations of the electric tie-line power, which benefits both the BIM and the utility grid.

2) The configuration of the energy management system of Microgrid (MEMS) and energy management systems of buildings (BEMSs) are presented and the interactions between the MEMS and BEMSs are also introduced. MEMS and BEMSs compute the hourly optimal schedules of DERs and smart buildings for daily operating cost reduction of the BIM based on the hourly day-ahead forecasting data at the first stage. Whereas at the second stage, the MEMS and BEMSs reschedule the DERs and the smart buildings to smooth the fluctuations of electric tie-line power of the BIM due to the errors of day-ahead forecasting data. The optimisation is done with information exchange between the two stages and the interactions between the MEMS and BEMSs.

3) A building is simplified to a lumped thermal mass and modelled as a simplified thermal storage system, namely the virtual energy storage system (VESS), which is scheduled as a flexible resource to fully explore the flexibility of the building with its thermal mass.

4) To improve the control performance in a time-varying context with uncertainties associated to forecasting data, the MPC based scheduling method is used at the intra-hour adjustment stage. By using the iterative rolling optimisation with finite horizon instead of the traditional open-loop and single-period based optimisation, the problems of the insufficient adjustments, excessive adjustments and untimely adjustments of the DERs and smart buildings at intra-hour stage can be solved.

5) Various practical constraints from the buildings and the DERs are considered in the proposed scheduling method. Moreover, a Microgrid is a low-voltage distribution network that is located down-stream of a distribution substation through a point of common coupling. Therefore, power flow and system operational constraints of the electric network of the Microgrid are also considered in the proposed scheduling model.

6) The proposed scheduling method provides a flexible energy management platform for BIM, which can be extended for optimal scheduling for other energy resources, such as electric vehicles. As a flexible resource, the integration of electric vehicles to the building is creating new opportunities for the Microgrid energy management. The electric vehicles integrated to the building can be modelled as

an aggregated DER under the Vehicle-to-Building (V2B) concept [31]. Then, the EVs can be scheduled as another DER with the proposed scheduling method.

The structure of this paper is summarized as follows. In Section 2, the system description and the mathematical model of the BIM is presented. Section 3 presents a detailed description and the mathematical model of the proposed multi-time scale and model predictive control based scheduling method. Section 4 discusses the scheduling results of the BIM in both scheduling stages and demonstrates the effectiveness of the proposed method by carrying out several comparative scenarios. Finally, Section 5 concludes the whole paper.

## 2. Configuration and modelling of an BIM

### *2.1. Configuration of the BIM*

The physical configuration of an BIM is shown in Fig. 1, mainly including multiple smart buildings, DERs (i.e., controllable DGs and battery), the MEMS and BEMSs installed in each smart building. The energy systems of a smart building include an electric chiller for cooling purpose, the renewable generations and other electric appliance. The proposed optimal scheduling method is based on information exchange between the MEMS and the BEMSs thanks to the communication infrastructure of the BIM. The functions of the MEMS and BEMS are described as follows:

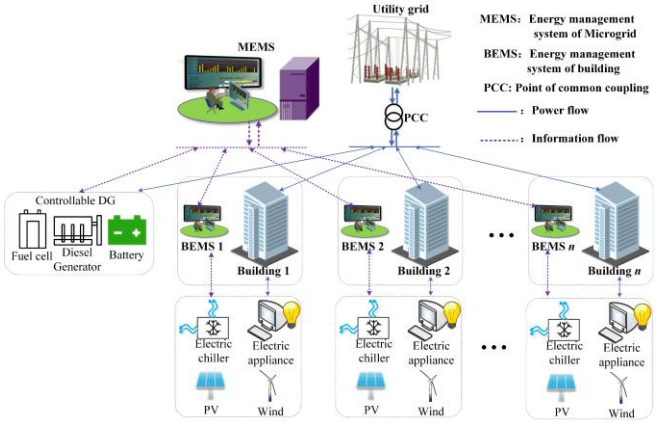


***Fig. 1.*** *Configuration of the BIM*

**MEMS:** MEMS monitors the energy consumption of buildings and interacts with every BEMS to optimise their energy usage within the user's comfort range. With the proposed scheduling method and the forecasting data from the BEMSs, optimal schedules of the DERs and the smart buildings are obtained and issued to the corresponding DG controllers and the BEMSs. The optimal schedules of the DERs include operational schedules at day-ahead stage, i.e., the unit commitment of the DGs and the charging/discharging schedules of the battery, and adjustment reschedules at intra-hour stage, i.e., the optimal adjustments of power outputs of the DGs and the charging/discharging power of the battery. The optimal schedules of each smart buildings at both stages are the optimised power consumption profiles of the electric chiller, which are used as control variables to fully explore the flexibility of the buildings.

**BEMS:** Forecasting data of solar radiation and outdoor temperature is obtained by BEMS from the weather station through the communication links. Meanwhile, the forecasting data of each building, i.e., electric power consumption of the electric appliance and internal heat gain, are obtained by BEMSs. All the forecasting data from BEMSs are uploaded to the MEMS. With the optimised load profile of each building issued by the MEMS and thermal model of the building, the indoor temperature schedules for each building are calculated by the BEMS and issued to the indoor temperature controller.

**Communication infrastructure**: For the optimal scheduling method, a bidirectional communication infrastructure is required between the BEMSs and the MEMS, as shown in Fig. 1. Also, unidirectional communication links are required between the BEMSs and the market operator, BEMSs and local weather station, MEMS and the DG controllers.

The smart buildings investigated in this paper are assumed to be public buildings that are centrally managed by a single public authority. Since the public buildings have the common interest of reducing the overall operating cost of the BIM, a centralized scheduling method is used in this paper. Future research will develop a decentralized scheduling method for private buildings that aims to minimise their own energy consumption and costs.

### *2.2. Components modelling*

*2.2.1 Building model:* Considering a summer cooling scenario, a building is modeled as a single isothermal air volume [32]. The mathematical relationship among the indoor temperature, cooling demand and outdoor temperature is formulated to investigate the thermal performance of a building by using the building thermal equilibrium equation, as shown in Eq. (1) [33].

$$\rho \times C \times V \times \frac{dT_{in}}{dt} = \dot{Q}_{wall} + \dot{Q}_{win} + \dot{Q}_{in} + \dot{Q}_{sw} + \dot{Q}_{sg} - \dot{Q}_{EC} \quad (1)$$

(i) $\dot{Q}_{wall}$ is calculated by summing the contribution of each wall of a building, as shown in Eq. (2). The roof of a building is accounted for as part of the external walls [34].

(ii) $\dot{Q}_{win}$ is calculated by summing the contribution of each window of a building, as shown in Eq. (3).

(iii) $\dot{Q}_{in}$ is the internal heat gains (kW).

(iv) $\dot{Q}_{sw}$ is calculated by summing the heat contribution due to solar radiation on each external wall (south, west, north and east orientations) according to the ISO 13790 [35], as shown in Eq. (4). Also, the external surface heat resistance for convection and radiation of the external wall $j$, $R_{se,j}$, is considered in Eq. (4). A typical method to calculate the $R_{se,j}$ is given in [36], which takes both radiation and convection terms into account.

(v) $\dot{Q}_{sg}$ is calculated according to Eq. (5). It is assumed that the total windows surfaces are distributed in the south, west, north and east orientations of the walls in a building uniformly [37].

(vi) $\dot{Q}_{EC}$ is the cooling power generated by the cooling equipment (kW).

$$\dot{Q}_{wall} = \sum_{j \in J} U_{wall} \times F_{wall,j} \times (T_{out} - T_{in}) \quad (2)$$

$$\dot{Q}_{win} = \sum_{j \in J} U_{win} \times F_{win,j} \times (T_{out} - T_{in}) \quad (3)$$

$$\dot{Q}_{sw} = \sum_{j \in J} \alpha_w \times R_{se,j} \times U_{wall} \times F_{wall,j} \times I_{T,j} \quad (4)$$

$$\dot{Q}_{sg} = \sum_{j \in J} \tau_{win} \times SC \times F_{win,j} \times I_{T,j} \quad (5)$$

$I_{T,j}$ is determined according to the method presented in Duffie and Beckman [38], which is a commonly used method to calculate the total solar radiation on a tilted surface [39]. It can be calculated as sum of various type of solar radiation, i.e., beam, diffuse and reflected radiation, as shown in Eq. (6):

$$I_T = I_b \times R_b + I_d \times \left(\frac{1+\cos\beta}{2}\right) + I \times \rho_g \times \left(\frac{1-\cos\beta}{2}\right) \quad (6)$$

where $I_b$, $I_d$ and $I$ represent beam, diffuse and total radiation on horizontal surface respectively (kW/m$^2$); $\rho_g$ is the ground reflectance and is taken as 0.2 in the present study [39]; $R_b$ is geometric factor which is defined as the ratio of beam radiation on a tilted surface to that on a horizontal surface, which is expressed as:

$$R_b = \frac{\cos\theta}{\cos\theta_z} \quad (7)$$

where $\theta$ and $\theta_z$ are incidence and zenith angles.

The thermal mass of a building can provide inertia. Like other technologies to store energy, this inherent property can be used to store energy at peak periods and preheat or precool the building without any additional investment cost. Therefore, the model of VESS is developed considering this inherent property of a building. The basic idea of the VESS is that the cooling demand of the building can be adjusted in the energy management process without disturbing the temperature comfort level due to the thermal mass of the building. Therefore, the cooling energy generated by the electric chiller is stored in the building when the electricity price is low, i.e., the electric chiller is started in advance or the power consumption of the electric chiller is increased. In that case, the VESS is charged seen from the Microgrid, i.e., $\dot{Q}'_{cl,building} < \dot{Q}_{cl,building}$. In the same way, the cooling energy generated by the electric chiller is discharged in the building when the electricity price is high, i.e., the electric chiller is shut down in advance or the power consumption of the electric chiller is decreased. In that case, the VESS is discharged seen from the Microgrid, i.e., $\dot{Q}'_{cl,building} > \dot{Q}_{cl,building}$. The charging/discharging power of the VESS, as shown in Eq. (8), is obtained following Eq. (1). The indoor temperature comfort zone and temperature set-point are considered in the model of VESS to maintain the customer comfort level.

$$\dot{Q}_{VESS,t} = \dot{Q}'_{cl,building,t} - \dot{Q}_{cl,building,t} \quad (8)$$

*2.2.2 Mathematical models of DER:*

1) Diesel engine

For diesel engine, the fuel cost depends on the power generation and fuel cost coefficients, which is shown in Eq. (9).

$$f_{fuel}(P_{DE,t}) = aP_{DE,t}^{\ 2} + bP_{DE,t} + c \quad (9)$$

2) Fuel cell

For fuel cell, the fuel cost depends on the power generation and efficiency $\eta_{FC}$, which is shown in Eq. (10).

$$f_{fuel}(P_{FC,t}) = C_{gas} \times P_{gas} = C_{gas} \times \left(P_{FC,t}\Delta t / \eta_{FC}\right) \quad (10)$$

3) Electric chiller

The electricity consumption of the electric chiller is determined by the cooling demand and the coefficient of performance, as shown in Eq. (11).

$$Q_{EC,t} = P_{EC,t} \times EER_{EC} \quad (11)$$

4) Battery

The state of charge (SOC) of the battery refers to the ratio of the residual energy to the rated energy. The SOC at dispatch time interval $t$ is described in Eq. (12).

$$SOC_t = \begin{cases} SOC_{t-1}(1-\delta) - P_{bt,t}\Delta t\eta_{ch} / CAP_{bt} & P_{bt,t} \le 0 \\ SOC_{t-1}(1-\delta) - P_{bt,t}\Delta t / (\eta_{dis} CAP_{bt}) & P_{bt,t} > 0 \end{cases} \quad (12)$$

## 3. The multi-time scale and model predictive control based scheduling method

### 3.1. Framework of the scheduling method

The proposed scheduling method is illustrated in Fig. 2, which includes two stages as introduced in the following text.

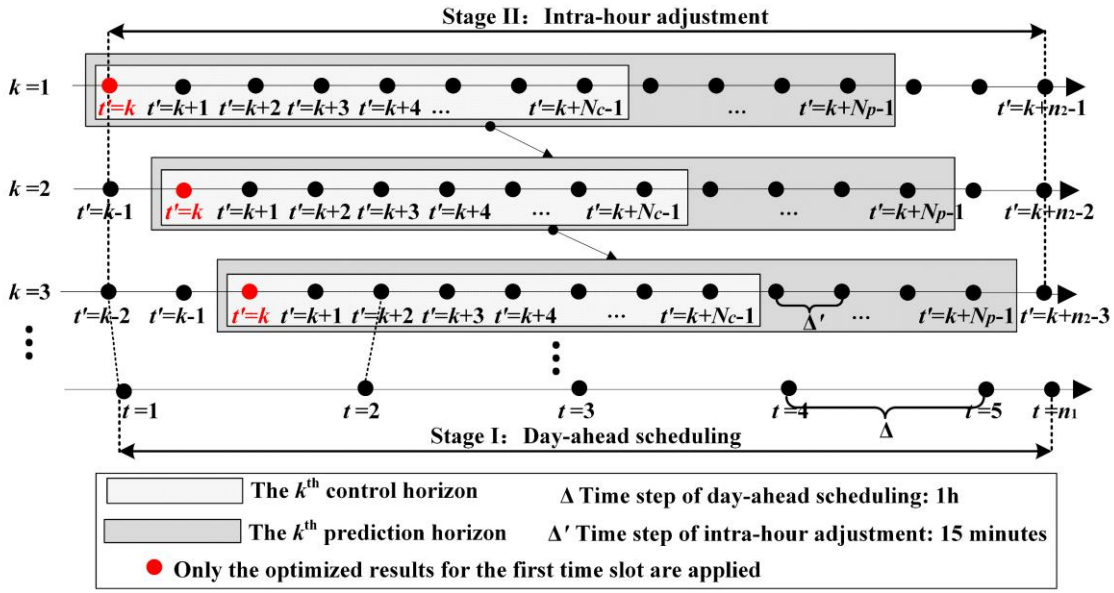


***Fig. 2.*** *Schematic illustration of the scheduling method*

*3.1.1 Day-ahead dynamic optimal scheduling stage:* With the hourly electric load demand, outdoor temperature, solar radiation and the renewable generation forecasting values, the hourly schedules at day-ahead stage over the $n_1$ time slots are obtained by the MEMS and the BEMSs. This stage works at a slow time scale, namely $\Delta t$. The hourly schedules include optimal schedules of the smart buildings (i.e., the optimized power consumption profiles of the electric chiller and the indoor temperature schedules), optimal schedules of the DREs (i.e., unit commitment of the

DGs and the charging/discharging schedules of the battery) and day-ahead set-points of electric tie-line power.

*3.1.2 Intra-hour rolling adjustment stage:* Based on the day-ahead schedules, computed at the beginning of each scheduling day, a reference profile of the power exchange with the utility grid for the full day ahead is agreed with the utility grid and should be followed to avoid penalties and additional cost. Due to the forecasting errors of the day-ahead forecasting data, there are errors between the schedules of the BIM at day-ahead stage and intra-hour stage. This induces fluctuations of the electric tie-line power of the BIM. Therefore, an MPC based two-layer intra-hour adjustment stage is conducted to smooth the fluctuations of the electric tie-line power. Faster-time scale is set in this stage with a shorter time step $\Delta t'$. As shown in Fig. 2, $\Delta t$ is further divided into four steps with an interval of $\Delta t'$. The whole scheduling time-line at intra-hour stage is divided into $n_2$ time slots and each time slot is allocated with 15 minutes.

The MPC based intra-hour rolling adjustment approach works as follows: At current time slot $t'=k$ & $k=1$, the BEMSs and MEMS get the current forecasting data over the time horizon from $k$ to $k+N_p$-1 (i.e., the $k^{\text{th}}$ prediction horizon). The MEMS then solves a forward-looking optimisation problem to minimise the errors between the tie-line power at day-ahead stage and intra-hour stage over the $N_c$-slot time horizon (i.e., the $k^{\text{th}}$ control horizon). The optimised results are a sequence of adjustments of power output of the DGs, charging/discharging power of the battery and the power consumption of the electric chillers. Only the optimised results for the first-time slot at $t'$, as highlighted in red in Fig. 2, are applied on the MEMS and issued to the corresponding DG controllers and the BEMSs. The unit commitment of the DGs and the charging/discharging status of the battery at intra-hour stage are kept the same with that at day-ahead stage. Then at next time slot $t'=k$ & $k=2$, the BEMSs and MEMS get updated forecasting data for the next $N_p$ time slots and the forward-looking optimisation problem over the next control horizon again is solved again. And the optimized results for the first-time slot are applied as the optimal adjustments for current time slot. The time horizon moves forward by one-time slot for the new forward-looking optimisation until all the control schedules are determined during the whole time-line.

The current state of the BIM at each time slot is used as the initial set points of the MPC at each time slot in this paper, which is a commonly used method to determine the initial set points of the MPC [40]. The current state of the BIM is determined as follows: At each time slot (i.e., $t'=k$ & $k\neq1$), the current state of the BIM is updated according to the prediction model of the BIM (as formulated in Section 3.3.1) and the information of state-space of the BIM at previous time slot (i.e., $t'=k$-1). At the first time slot (i.e., $t'=k$ & $k=1$), the current state of the BIM cannot obtained according to the prediction model of the BIM due to lack of the information of state-space of the BIM at previous time slot. Therefore, the day-ahead scheduling results at the first time slot of the day-ahead stage is used as the initial set points for MPC at the first time slot of the intra-hour stage.

### *3.2. Formulation of the scheduling method: Stage I*

With the hourly electric load demand, outdoor temperature, solar radiation and the renewable generation forecasting values, the hourly schedules of the day-ahead stage over the horizon $T = \{t=1, t=2, \ldots, t=n_1\}$ are obtained by using an optimal dynamic scheduling program. The optimisation problem of stage I is formulated as follows.

*3.2.1 Objective function:* The objective function depicted in Eq. (13) is to minimise the total daily operating cost for the BIM.

$$\min \sum_{t\in T}\Bigg\{\left(\frac{C_{ph,t}+C_{se,t}}{2}P_{grid,t}+\frac{C_{ph,t}-C_{se,t}}{2}\left|P_{grid,t}\right|\right) + \left(\sum_{i\in DG}\left[f_{fuel}\left(P_{DG,i,t}\right)+\rho_{DG,i}\times P_{DG,i,t}+\rho_{su,i}\times U'_{DG,i,t}\right]\right) + \left(\rho_{WT}P_{WT,t}+\rho_{PV}P_{PV,t}+\rho_{bt}\left|P_{bt,t}\right|+\sum_{n\in EC}\rho_{EC}P_{EC,n,t}\right)\Bigg\} \quad (13)$$

The first term in Eq. (13) represents the cost for electricity purchase from the utility grid; The second term represents the fuel costs depicted by fuel cost function $f_{fuel}(\,)$, maintenance costs and the startup costs of all the controllable DGs; the third term is the maintenance costs of other devices of the BIM.

*3.2.2 Constraints:*

(1) Constraints of the Microgrid

- *Electrical power balance:*

$$P^{dh}_{grid,t}+\sum_{i\in DG}P_{DG,i,t}+P_{WT,t}+P_{PV,t}+P_{bt,t}-\sum_{m\in BD}P_{el,m,t} -P_{load,t}-\sum_{n\in EC}P_{EC,n,t}-P_{loss,t}=0 \quad \forall t\in T \quad (14)$$

- *Constraint of electric power exchange*

$$\underline{P_{grid}}<P^{dh}_{grid,t}<\overline{P_{grid}} \quad ,\forall t\in T \quad (15)$$

- *Power flow equations:*

$$\begin{cases} P_{t,i}-\sum\limits_{\substack{f_e\in N_{br}\\ j\in N_{e\text{-}bus}}}P^{f_e}_{t,ij}\left(V_i,V_j,Y_{ij},\theta_{ij}\right)=0 \quad \forall t\in T \\ Q_{t,i}-\sum\limits_{\substack{f_e\in N_{br}\\ j\in N_{e\text{-}bus}}}Q^{f_e}_{t,ij}\left(V_i,V_j,Y_{ij},\theta_{ij}\right)=0 \quad \forall t\in T \end{cases} \quad (16)$$

where $P_{t,i}$ and $Q_{t,i}$ are the net injected active and reactive powers at the $i^{\text{th}}$ electric bus at time $t$.

- *Constraint of electric network*

$$\begin{cases} V_{\min}\le V_i^a\le V_{\max} \\ V_{\min}\le V_i^b\le V_{\max} \\ V_{\min}\le V_i^c\le V_{\max} \end{cases} \quad (17)$$

$$i^{f_e}_{t,ij}\le i^{f_e}_{ij,\max} \quad (18)$$

$$N_{loop}=N_{br}-N_{e\text{-}bus}+1 \quad (19)$$

Eq. (16) is the electric power flow equation; Eq. (17) is the three-phase bus voltage constraint of the electric distribution network; Eq. (18) is the current constraint of the electric feeder; Eq. (19) is established to guarantee that the electric network has a radial structure.

(2) Constraints of the DERs

- *Constraint of DGs*

In the dynamic scheduling model, the constraints from the controllable DGs are introduced to consider the inherent link among the scheduling time intervals. For each controllable DG, the power generation is constrained by the upper and lower power output limits; The power generations between two successive dispatch time intervals are

constrained by ramp-up (ramp-down) rates as well as startup (shutdown) rates, as shown in Eq. (20):

$$\begin{cases} \underline{P}_{DG,i,t} U_{DG,i,t} \le P_{DG,i,t} \le \overline{P}_{DG,i,t} U_{DG,i,t} \\ P_{DG,i,t} - P_{DG,i,t-1} \le R_{u,i} \Delta t U_{DG,i,t-1} + S_{u,i} \Delta t U'_{DG,i,t} \\ P_{DG,i,t-1} - P_{DG,i,t} \le R_{d,i} \Delta t U_{DG,i,t} + S_{d,i} \Delta t U''_{DG,i,t} \\ U'_{DG,i,t} = \max\left(0, U_{DG,i,t} - U_{DG,i,t-1}\right) \\ U''_{DG,i,t} = \max\left(0, U_{DG,i,t-1} - U_{DG,i,t}\right) \\ \forall i \in DG, \forall t \in T \end{cases} \quad (20)$$

The controllable DGs are also constrained by the minimum up and down time limits, as shown in Eq. (21).

$$\begin{cases} T_{i,t}^{on} \ge UT_i \left(U_{DG,i,t} - U_{DG,i,t-1}\right) \\ T_{i,t}^{off} \ge DT_i \left(U_{DG,i,t-1} - U_{DG,i,t}\right) \\ \forall i \in DG, \forall t \in T \end{cases} \quad (21)$$

- *Constraint of the battery*

For the battery, the charging/discharging power and the SOC are constrained by the upper and lower limits shown in Eqs. (22) ~ (24); For the energy balance, the stored energy inside the battery is set the same as the initial stored energy, as shown in Eq. (25).

$$\underline{P}_{bt} \le P_{bt,t} \le \overline{P}_{bt} \quad , \forall t \in T \quad (22)$$

$$\underline{SOC} \le SOC_t \le \overline{SOC} \quad , \forall t \in T \quad (23)$$

$$SOC_t = \frac{E_{bt,t}}{CAP_{bt}} \quad (24)$$

$$\sum_{t \in T} \boldsymbol{P}_{bt,t} = 0 \quad (25)$$

- *Constraint of the electric chiller*

$$0 \le Q_{EC,t} \le \overline{Q}_{EC}, \quad \forall t \in T \quad (26)$$

(3) Constraints of the buildings

- *Cooling demand balance*

$$\dot{Q}_{EC,t} = EER_{EC} \times P_{EC,t} = \dot{Q}_{cl,building,t}, \quad \forall t \in T \quad (27)$$

- *Building thermal equilibrium equation*

$$\Delta t \left[\dot{Q}_{wall,t} + \dot{Q}_{win,t} + \dot{Q}_{sw,t} + \dot{Q}_{sg,t} + \dot{Q}_{in,t} - \dot{Q}_{EC,t}\right] - \rho CV\left(T_{in,t+1} - T_{in,t}\right) = 0, \quad \forall t \in T \quad (28)$$

- *Indoor temperature set-point constraint*

$$\underline{T_{in}} < T_{in,t} < \overline{T_{in}}, \quad \forall t \in T \quad (29)$$

### 3.3. Formulation of the scheduling method: Stage II

The MPC strategy with operational constraints is proposed to reschedule the smart buildings and DERs at intra-hour stage. The BEMSs and the local controllers of the DERs not only have to consider local information, but also exchange the state information with the MEMS, as introduced in Section 2.1. Therefore, the prediction model of the BIM is developed to inform the MEMS, BEMSs and DER controllers for rescheduling of the smart buildings and DERs. Then, the rolling optimisation problem is formulated and the implementation of the MPC based rescheduling method is introduced.

#### 3.3.1 Prediction model:

(1) Prediction model of the Microgrid

According to the above system dynamics shown in Eqs. (1), (12) and (20), constraints of the Microgrid, DERs and smart buildings, as introduced in Section 3.2.2, the prediction model of the BIM is formulated using state-space, as shown in Eq. (30). The state of the Microgrid can be predicted by the iteration for the state-space model repeatedly with the updated forecasting data.

$$\begin{cases} \boldsymbol{x}(t'+1) = A \cdot \boldsymbol{x}(t') + B \cdot \boldsymbol{u}(t') + C \cdot \boldsymbol{r}(t') \\ \boldsymbol{y}(t') = D \cdot \boldsymbol{x}(t') \end{cases} \quad (30)$$

where

$$\boldsymbol{x}(t') = \left[P_{grid}(t'), \boldsymbol{P_{DG}}(t'), P_{bt}(t'), SOC(t'), \boldsymbol{P_{EC}}(t')\right]^{\mathrm{T}} \quad (31)$$

$$\boldsymbol{u}(t') = \left[\boldsymbol{\Delta P_{DG}}(t'), \Delta P_{bt}(t'), \boldsymbol{\Delta P_{EC}}(t')\right]^{\mathrm{T}} \quad (32)$$

$$\boldsymbol{r}(t') = \left[\Delta P_{PV}(t'), \Delta P_{WT}(t'), \boldsymbol{\Delta P_{el}}(t')\right]^{\mathrm{T}} \quad (33)$$

$$\boldsymbol{y}(t') = P_{grid}(t') \quad (34)$$

Here $\boldsymbol{x}(t')$ is the state vector of the BIM at current time slot $t'$, which consists of power exchange with the utility grid ($P_{grid}(t')$), vector of power output of controllable DGs ($\boldsymbol{P_{DG}}(t')$), charging/discharging power of the battery ($P_{bt}(t')$) and its SOC value ($SOC(t')$), vector of power consumption of electric chillers ($\boldsymbol{P_{EC}}(t')$). $\boldsymbol{u}(t')$ is the control vector of the BIM at current time slot $t'$, which manages the increments of $\boldsymbol{P_{DG}}(t')$, $P_{bt}(t')$ and $\boldsymbol{P_{EC}}(t')$, as shown in Eq. (32). The unit commitment of the controllable DGs and the charging/discharging modes of the battery at intra-hour stage are kept the same with that at day-ahead stage. Therefore, they are not managed and controlled at intra-hour stage. $\boldsymbol{r}(t')$ is the input vector that influences the BIM at current time slot $t'$, which consists of day-ahead forecasting errors of PV generation ($\Delta P_{PV}(t')$), wind generation ($\Delta P_{WT}(t')$) and electric loads of the buildings ($\boldsymbol{\Delta P_{el}}(t')$). $y(t')$ is the output of the prediction model of the Microgrid at current time slot $t'$, which is the power exchange with the utility grid ($P_{grid}(t')$). The matrices $A$, $B$, $C$ and $D$ are the relevant state-space matrices, as shown in Eqs. (35)-(38):

$$A = \begin{bmatrix} 1 & 0 & 0 & 0 & 0 \\ 0 & E_n & 0 & 0 & 0 \\ 0 & 0 & 1 & 0 & 0 \\ 0 & 0 & \boldsymbol{\varphi} & 1-\boldsymbol{\delta} & 0 \\ 0 & 0 & 0 & 0 & E_m \end{bmatrix} \quad (35)$$

$$B = \begin{bmatrix} -1 & -1 & 1 \\ E_n & 0 & 0 \\ 0 & 1 & 0 \\ 0 & \boldsymbol{\varphi} & 0 \\ 0 & 0 & E_m \end{bmatrix} \quad (36)$$

$$C = \begin{bmatrix} -1 & -1 & E_n \\ 0 & 0 & 0 \\ 0 & 0 & 0 \\ 0 & 0 & 0 \\ 0 & 0 & 0 \end{bmatrix} \quad (37)$$

$$D = \begin{bmatrix} 1 & \mathbf{0} & 0 & 0 & \mathbf{0} \end{bmatrix} \quad (38)$$

where $E_n$ and $E_m$ are identity matrices; $\varphi$ is the recurrence coefficient for SOC value calculation of the battery, as shown in Eq. (39).

$$\boldsymbol{\varphi} = \begin{cases} -\dfrac{\Delta t \eta_{ch}}{CAP_{bt}} & P_{bt,t} \le 0 \\ -\dfrac{\Delta t}{\eta_{dis} CAP_{bt}} & P_{bt,t} > 0 \end{cases} \tag{39}$$

According to the model in Eq. (30), the predicted output of the Microgrid at time slot $t'+p$, can be calculated by the iteration based on the state at time slot $t'$, as shown in Eq. (40):

$$\begin{aligned} \boldsymbol{y}(t'+p \mid t') &= D \cdot \boldsymbol{x}(t'+p \mid t') = D \cdot \left[ A^{p} \cdot x(t') \right. \\ &+ A^{p-1} B \cdot u(t') + A^{p-1} C \cdot r(t') + ..., \\ &\left. + B \cdot u(t'+p-1 \mid t') + C \cdot r(t'+p-1 \mid t') \right] \end{aligned} \tag{40}$$

Then, the predicted output of the Microgrid over the $k^{\text{th}}$ prediction horizon can be formulated by the augmented vector, as shown in Eq. (41).

$$\begin{aligned} &\boldsymbol{Y} = \left[ \boldsymbol{y}(k \mid k), \boldsymbol{y}(k+1 \mid k), ..., \boldsymbol{y}(k+N_p-1 \mid k) \right]^{\mathrm{T}}, \\ &k = 1, 2, ..., n_2 \end{aligned} \tag{41}$$

(2) Prediction model of indoor temperatures of a building

The recurrence equation to predict the indoor temperature of a building can be obtained according to the building model, as shown in Eq. (42).

$$T_{in}(t'+1) - T_{in}(t') = \frac{\Delta t (\hat{Q}_{wall} + \hat{Q}_{win} + \hat{Q}_{sw} + \hat{Q}_{sg} + \hat{Q}_{in} - \hat{Q}_{EC})}{\rho C V} \tag{42}$$

$\hat{Q}$ is the updated value with the updated forecasting data of a building ($\lambda(t')$). $\lambda(t')$ consists of forecasting errors of internal heat gain ($\Delta \dot{\boldsymbol{Q}}_{in}(t')$), outdoor temperature ($\Delta T_{out}(t')$) and solar radiation ($\Delta I_T(t')$):

$$\lambda(t') = [\Delta \dot{\boldsymbol{Q}}_{in}(t'), \Delta T_{out}(t'), \Delta I_T(t')] \tag{43}$$

According to Eqs. (42) and (43), the indoor temperature of a building can be predicted by the iteration for the recurrence equation repeatedly with the updated forecasting data and the prior knowledge of state information of the Microgrid, as shown in Eq. (30) and (41).

*3.3.2 Rolling optimisation*: The objective is to keep the predicted output of the Microgrid, i.e., power exchange with the utility grid $P_{grid}(t')$, close to the day-ahead schedules at each control horizon. The predicted output of the Microgrid over the $k^{\text{th}}$ control horizon is shown in Eq. (44).

$$\begin{aligned} &\boldsymbol{Y} = \left[ \boldsymbol{y}(k \mid k), \boldsymbol{y}(k+1 \mid k), ..., \boldsymbol{y}(k+N_c-1 \mid k) \right]^{\mathrm{T}}, \\ &k = 1, 2, ..., n_2 \end{aligned} \tag{44}$$

The day-ahead schedules of the power exchange with the utility grid over the $k^{\text{th}}$ control horizon are generated in stage I and described as augmented vector, as shown in Eq. (45).

$$\begin{aligned} &\boldsymbol{Y}_{dh} = \left[ P_{grid}^{dh}(k \mid k), P_{grid}^{dh}(k+1 \mid k), ..., P_{grid}^{dh}(k+N_c-1 \mid k) \right]^{\mathrm{T}}, \\ &k = 1, 2, ..., n_2 \end{aligned} \tag{45}$$

Then the optimisation problem for each control horizon can be formulated as:

$$\begin{aligned} \min \quad & f = \left( \boldsymbol{Y}_{dh} - \boldsymbol{Y} \right)^{\mathrm{T}} \left( \boldsymbol{Y}_{dh} - \boldsymbol{Y} \right) \\ & + \sum_{t'=k}^{t'=k+N_c-1} \boldsymbol{\theta}_{bt} \left[ \left( \Delta P_{bt}(t') \right)^2 \right] \cdot \Delta t' \\ s.t. \quad & (14) - (29) \end{aligned} \tag{46}$$

where $\boldsymbol{\theta}_{bt}$ is the penalty coefficient that limits the frequent charge and discharge operation of the battery. By adding the penalty item on the objective function, the SOC values of the battery at stage II would follow that at stage I as close as possible.

*3.3.3 Implementation process*: In stage I, a day-ahead dynamic optimiser is designed at a slow time scale. The optimal day-ahead schedules are decided by running the dynamic optimisation problem with day-ahead forecasting data. In stage II, an intra-hour rescheduling method with faster time scale is proposed using MPC strategy. The mismatch between supply and demand due to forecasting errors is compensated by rescheduling the DERs and the smart buildings. Furthermore, a two-layer framework is specifically designed to coordinate and manage the MEMS, BEMSs and DG controllers effectively in stage II. Following the details introduced in Sections 3.2 and 3.3, the proposed scheduling method for the BIM can be realized by Algorithm 1 and its flowchart is shown in Fig. 3.

***Algorithm 1*** The multi-time scale and model predictive control based scheduling method.

➢ ***Stage I: Day-ahead dynamic optimisation***
**Set** sample interval $\Delta t$ = 1 h; $t$ = 1; run time $n_1$ = 24.
**Take** day-ahead forecasting data over the whole scheduling day:
$\mathbb{Z}_t = \left[ \boldsymbol{P}_{el}(t)^T \boldsymbol{T}_{out}(t)^T \boldsymbol{I}_T(t)^T \dot{\boldsymbol{Q}}_{in}(t)^T \boldsymbol{P}_{WT}(t)^T \boldsymbol{P}_{PV}(t)^T \right]^T$, $t$ = 1, 2, …, $n_1$.
**Solve** the dynamic optimisation problem in (13), subject to the constraints (14)-(29).
**Output** the day-ahead schedules of the BIM.
➢ ***Stage II: Intra-hour rescheduling optimisation***
**Set** sample interval $\Delta t'$ = 0.25 *h*; prediction horizon $N_p * \Delta t'$= 4 *h*; control horizon $N_c * \Delta t'$= 4 *h*; $k$ = 1; run time $n_2$ = 96.
**for** $k$ = 1 : $n_2$ **do**
  **Set** current time $t' = k$.
  ***The master level: MEMS***
  **Take** the updated forecasting data over the $k^{\text{th}}$ prediction horizon:
  $\mathbb{Z}_{t'} = \left[ \boldsymbol{P}_{el}(t')^T \boldsymbol{T}_{out}(t')^T \boldsymbol{I}_T(t')^T \dot{\boldsymbol{Q}}_{in}(t')^T \boldsymbol{P}_{WT}(t')^T \boldsymbol{P}_{PV}(t')^T \right]^T$, $t' = k$, $k$+1, …, $k$+$N_p$-1.
  **Predict** the output of the Microgrid over the $k^{\text{th}}$ control horizon based on the prediction model of the Microgrid in (30).
  **Collect** the operational parameters of buildings and controllable DGs.
  **Solve** the rescheduling optimisation problem in (46) for the $k^{\text{th}}$ control horizon, subject to the constraints (14)-(29).
  **Output** the optimal schedules over the $k^{\text{th}}$ control horizon:
  $\boldsymbol{u}(t') = \left[ \Delta \boldsymbol{P}_{DG}(t'), \Delta P_{bt}(t'), \Delta \boldsymbol{P}_{EC}(t') \right]^T$ $t' = k, k+1, \ldots, k+N_c-1$.
  **Apply** the optimized schedules for the current time step $t' = k$ on the MEMS and issue the results to BEMSs and DG controllers.
  ***The client level: BEMS of each building***
  **Obtain** the adjustment command for the electric chiller $\Delta \boldsymbol{P}_{EC}(t')$ at current time step $t' = k$.
  **Obtain** the indoor temperature set-points based on $\Delta P_{EC}(t')$ and the recurrence equation in (42).
  **Apply** the indoor temperature set-points on the heating, ventilation and air-conditioning systems.
  ***The client level: DG controllers***
  **Obtain** the adjustment command for the DGs $\Delta \boldsymbol{P}_{EC}(t')$ and battery $\Delta P_{bt}(t')$ at current time step $t' = k$.
  **Apply** the adjustment command on the DG controllers.
  $k \leftarrow k$+1 and go to step 7.
**end**

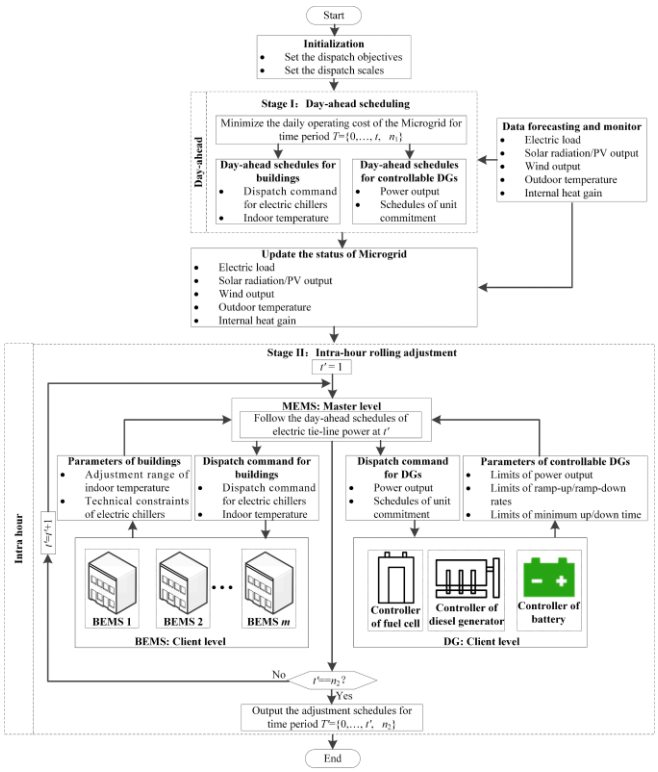


***Fig. 3.*** *Flowchart of the scheduling method*

*3.3.4 Solution algorithm*: In this paper, the optimal scheduling problem is solved by using a co-simulation platform, as shown in Fig. A1 of Appendix A. The co-simulation platform consists of three modules, i.e., formulation and modelling module in MATLAB, optimisation solver in IBM ILOG CPLEX [41] and power flow calculation in OpenDSS [42]. The formulation of the optimisation problem (i.e., the objective functions and the constraints) and the model of the BIM (i.e., the building model, models of DGs and the Microgrid model) are implemented in MATLAB; MATLAB routes the optimisation model to the solver – IBM ILOG CPLEX Optimizer to solve the optimal scheduling problem; OpenDSS gets the optimal control variables from MATLAB and runs the sequential power flow of the electric network over successive time intervals. Then, the power loss is calculated while satisfying the network constraints of the Microgrid in OpenDSS. The principal procedure is described by Algorithm 2. This similar iteration-based algorithm has been applied on the optimal scheduling of an active distribution network [43] and an integrated community energy system [44].

**Algorithm 2** The implementation procedure of the optimisation.

**Set** iteration coefficient $IC_1 = IC_2 = 1$ and their maximum values $n_1$ and $n_2$; initial value of power loss $P_{loss}^0$; precision coefficient $e$; adjustment constant $\Delta \boldsymbol{P_e}$.
**for** $IC_2 = 1 : n_2$ **do**
  **for** $IC_1 = 1 : n_1$ **do**
    **Solve** the optimisation problem in CPLEX with $P_{loss}^0$.
    **Run** power flow in OpenDSS based on the optimal control variables $\boldsymbol{u} = [\boldsymbol{P_{DG}}, P_{bt}, \boldsymbol{-P_{EC}}]$, $\underline{\boldsymbol{u}} \le \boldsymbol{u} \le \overline{\boldsymbol{u}}$ generated by CPLEX.
    **Check** the feasibility of the optimal solution.
    **if** the lower limits of Eq. (17) are not satisfied or Eq. (18) is not satisfied **then**
      Update the lower limits of control variables: $\underline{\boldsymbol{u}} \leftarrow \underline{\boldsymbol{u}} + \Delta \boldsymbol{P_e}$.
      $IC_1 \leftarrow IC_1+1$ and go to step 4.
    **elseif** the upper limits of Eq. (17) are not satisfied **then**
      **Update** the upper limits of control variables: $\overline{\boldsymbol{u}} \leftarrow \overline{\boldsymbol{u}} - \Delta \boldsymbol{P_e}$.
      $IC_1 \leftarrow IC_1+1$ and go to step 4.
    **else**
      **break**
    **end if**
  **end for**
  **Calculate** the power loss $P_{loss}$ in OpenDSS.
  **if** the change of power loss $\Delta P_{loss} > e$ **then**
    $IC_2 \leftarrow IC_2+1$ and go to step 4 with the updated $P_{loss}$.
  **else**
    **break**
  **end if**
**end for**

## 4. Results and discussion

### *4.1. Case study*

A BIM shown in Fig. A2 of Appendix A containing smart buildings and DERs is used to verify the proposed scheduling method. Diesel engine 1, diesel engine 2, fuel cell, PV & battery and wind generator are connected to electric buses 680, 632, 633, 692 and 645 (B-phase), respectively. Four smart buildings are connected to electric buses 670, 671, 634 and 675, respectively. Day-ahead forecasting values of the outdoor temperature, solar radiations on horizontal surface, electric loads and internal heat gains of the four buildings, and renewable generations are shown in Figs. A3 - A5 of Appendix A. The capacity of the installed PV and wind based DGs are set to be 300 kW and 500 kW respectively. All day-ahead forecasting data are collected from [9]. The corresponding incident solar radiation on the walls/windows surface at south, west, north and east orientations are calculated based on the method presented by Duffie and Beckman, as shown in Fig. A3 of Appendix A. The electricity purchasing prices are shown in Fig. A6 of Appendix A, and the price for selling electricity back to the utility grid is set to be 0.8 times the price for purchasing electricity [10]. The short-term forecasting data over the prediction horizon at intra-hour stage need forecasting techniques, which are beyond the scope of this paper. Instead, we assume that the forecasting errors of all the data at intra-hour stage follows the uniform distribution [45]-[46], as shown in Eq. (47):

$$\begin{cases} P_{WT}(t') = P_{WT}(t) \cdot [1 + E_{WT}^{\max} \cdot R(t)] \\ P_{PV}(t') = P_{PV}(t) \cdot [1 + E_{PV}^{\max} \cdot R(t)] \\ P_{el}(t') = P_{el}(t) \cdot [1 + E_{el}^{\max} \cdot R(t)] \\ T_{out}(t') = T_{out}(t) \cdot [1 + E_{t}^{\max} \cdot R(t)] \end{cases} \quad (47)$$

where $E_{WT}^{\max}$, $E_{PV}^{\max}$, $E_{el}^{\max}$ and $E_{t}^{\max}$ are the threshold values of the forecasting errors under different uncertainty levels, and their values are listed in Tab. B1 of Appendix B; $R(t)$ is a random value that follows the uniform distribution: $R(t) \sim U(-1,1)$. In this study, the uncertainty level is considered as Level 1.

The building studied in this paper is represented by a parallelepiped with a squared floor. The thermal parameters and the occupied hours of the buildings are given in Tab. B2 of Appendix B [9]. The values of the parameters of the air mass density $\rho$ and air specific heat ratio $C$ are set to be 1.2kg/m$^3$ and 1000J/(kg·ºC) respectively. The acceptable indoor temperature set-point range for human occupancy in a building varies under different operational scenarios. In this study, the indoor temperature set-point during occupied hours is set to be 22.5 ºC without VESS being dispatched. The indoor temperature set-point range during occupied hours is set to be from 19 ºC to 26 ºC with VESS being dispatched. It is worth noting that the electric chillers of the buildings are

switched off during unoccupied hours for cost saving. In this context, the indoor temperatures are not optimised and no specific indoor temperature set-point range is assigned by the BEMSs during the unoccupied hours. The technical and economic parameters of the DERs are shown in Tabs. B3-B4 of Appendix B. The other operational parameters of the DERs are shown in Tab. B5 of Appendix B. The fuel cost coefficients of the diesel engine are set as: a=44 ($/h/MW2), b=65.34 ($/h/MW) and c=1.1825 ($/h). The natural gas price is 42.5$/MWh. All the parameters regarding the DERs are collected from Refs. [47]-[51].

### *4.2. Day-ahead scheduling results*

The day-ahead schedules of the DERs are shown in Fig. 4. The results show that all the controllable DGs are committed and dispatched at their maximum capacities during high electricity purchasing price periods (i.e., 11:00–12:00 & 14:00–18:00). They are switched off or the power generations are reduced for cost savings during low electricity purchasing price periods (i.e., 01:00–10:00 & 19:00–23:00). However, due to the constraint of electric power exchange, as shown in Eq. (15), required electric power cannot be imported from the utility grid at 08:00–10:00. Therefore, the fuel cell is committed and scheduled at 08:00–10:00 to cover the power shortage without VESSs' participation in day-ahead scheduling, as shown in Fig. 4(a) [1]. However, the cooling demands of the buildings are adjusted to reduce the power consumptions of the electric chillers considering VESSs' participation, which results in no power shortage at 08:00–10:00. Therefore, unit commitment of the DGs is not needed at 08:00–10:00 and more cost savings are achieved. The PV and wind based DGs are uncontrollable DGs. In this context, their power outputs are not optimised and scheduled by the MEMS. Therefore, the schedules of the PV and wind based DGs are not presented in Fig. 4.

The day-ahead cooling schedules of the buildings are shown in Fig. 5. We can observe that the indoor temperatures are adjusted within the indoor temperature comfort range (19 ºC - 26 ºC) during the occupied hours by introducing VESS to the day-ahead scheduling stage. The indoor temperatures are kept at the set-points (22.5 ºC) during the occupied hours without considering VESSs' participation. In this case, the daily operating cost of the BIM is reduced from $2128.9 to $2080.7, which is reduced by 2.3%. It can be concluded that the VESSs' participation in day-ahead scheduling can reduce the daily operating cost of the BIM with limited modifications on the Microgrid management system. The day-ahead schedules of VESSs are shown in Fig. A7 of Appendix A. More details regarding the schedules of VESSs and their relationship with electricity purchasing prices are referred to Ref. [9] due to the limited space.

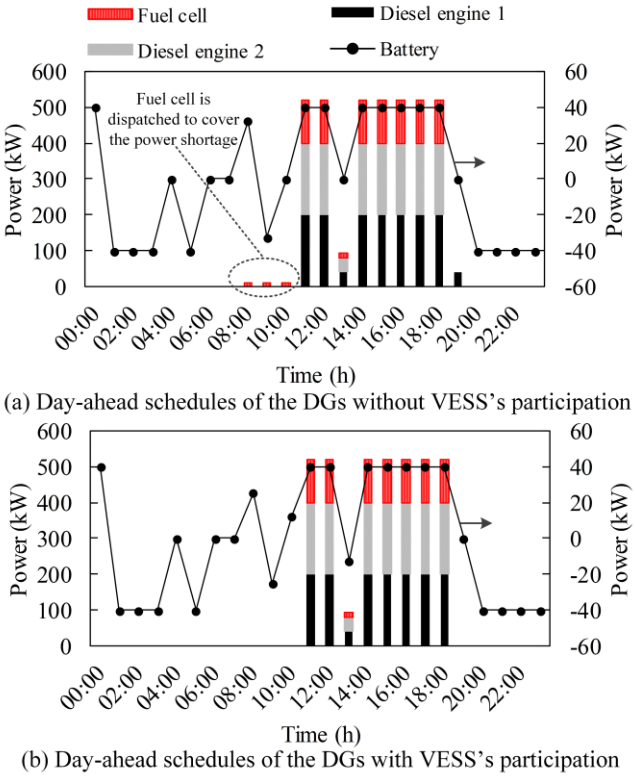

(a) Day-ahead schedules of the DGs without VESS's participation

(b) Day-ahead schedules of the DGs with VESS's participation

***Fig. 4.*** *Day-ahead schedules of the DERs*

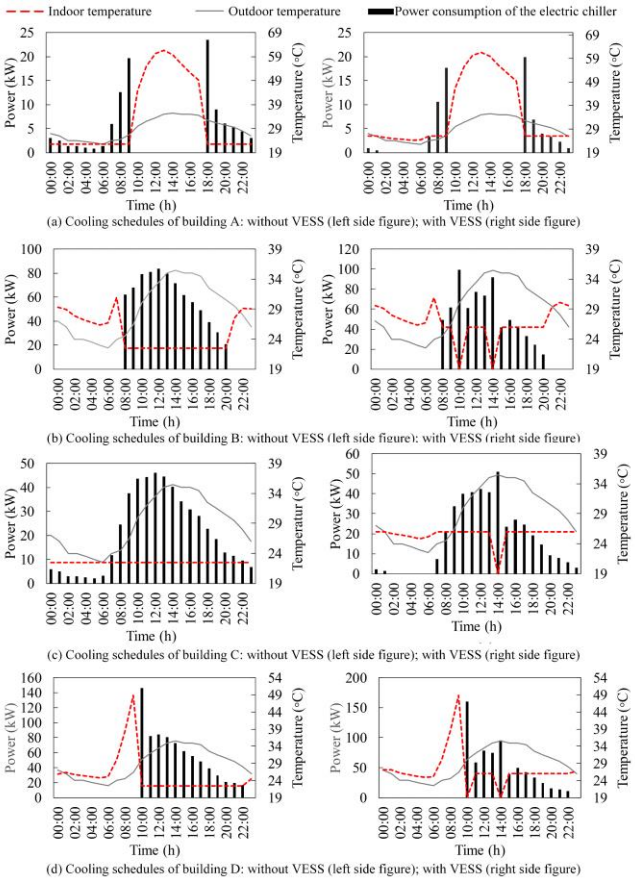

(a) Cooling schedules of building A: without VESS (left side figure); with VESS (right side figure)

(b) Cooling schedules of building B: without VESS (left side figure); with VESS (right side figure)

(c) Cooling schedules of building C: without VESS (left side figure); with VESS (right side figure)

(d) Cooling schedules of building D: without VESS (left side figure); with VESS (right side figure)

***Fig. 5.*** *Day-ahead cooling schedules of the buildings*

The three-phase voltages during one scheduling day are shown in Fig. 6 (a)-(c). It can be observed that the voltages of the network can satisfy the voltage limits (as shown in Eq.

[1] Only the fuel cell is scheduled at 08:00–10:00 because of its low-cost coefficient compared with the diesel engine.

(17)) using the proposed solution algorithm. The hourly power losses of the network at each iteration are shown in Fig. 6(d). Initially, the power losses are assumed to be zero. After 5 iterations, the power losses converge to the steady states and the optimal day-ahead schedules of the BIM are found.

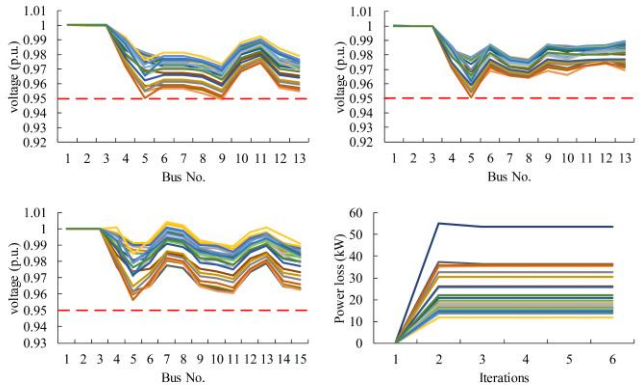


***Fig. 6.*** *Voltages and power losses of the network with VESSs' participation*

### *4.3. Intra-hour adjustment results*

The day-ahead programming (DA-P) strategy used in [9] and single-period based strategy used in [25] are employed to compare with the MPC based strategy developed in this paper. Then the effectiveness of the proposed MPC based energy management method in the intra-hour stage is further verified.

DA-P strategy [9]: The DERs and VESSs are not rescheduled under the DA-P strategy in the intra-hour stage. Therefore, the errors between the schedules of day-ahead stage and intra-hour stage caused by day-ahead forecasting errors would be balanced by the utility grid.

Single-period based strategy [25]: The DERs and VESSs are rescheduled to cope with the day-ahead forecasting errors in the intra-hour stage. However, the rescheduled results of the DERs and VESSs are optimised based on the operating status of the BIM and forecasting data at current operational period rather than the predictive operating status and forecasting data over a future time horizon.

Different from the DA-P strategy and the single-period based strategy, the MPC based strategy reschedule the DERs and VESSs based on the predictive operating status and forecasting data over a future time horizon that runs the embedded optimisation model repeatedly with updated forecasts. The prediction horizon and control horizon are set to be 4 h [28] (i.e., $N_p$=$N_c$=16) in the intra-hour adjustment stage in this paper.

Three comparative scenarios are carried out to verify the effectiveness of the proposed energy management method in the intra-hour stage. The DA-P strategy is named as Scenario I, single-period based strategy is named as Scenario II and the MPC based strategy is named as Scenario III.

**Scenario I (DA-P strategy)**: Dispatch the BIM using day-ahead programming (DA-P) method [9]. Mismatches between the energy demand and supply caused by day-ahead forecasting errors are balanced by the utility grid, without rescheduling the DERs and VESSs.

**Scenario II (Single-period based strategy)**: Reschedule the DERs and VESSs to cope with the day-ahead forecasting errors in the intra-hour adjustment stage using traditional single-period based optimisation strategy [25].

**Scenario III (MPC based strategy)**: Reschedule the DERs and VESSs to cope with the day-ahead forecasting errors in the intra-hour adjustment stage using MPC based optimisation strategy.

The electric tie-line powers of the BIM in the comparative scenarios are shown in Fig. 7 (a). Since all the mismatches between the energy demand and supply are balanced by electric power from the utility grid under the DA-P method in Scenario I, all the forecasting errors are mainly reflected in the electric tie-line power. The fluctuations of the electric tie-line power can be smoothed by rescheduling the DERs and VESSs in Scenario I and Scenario II.

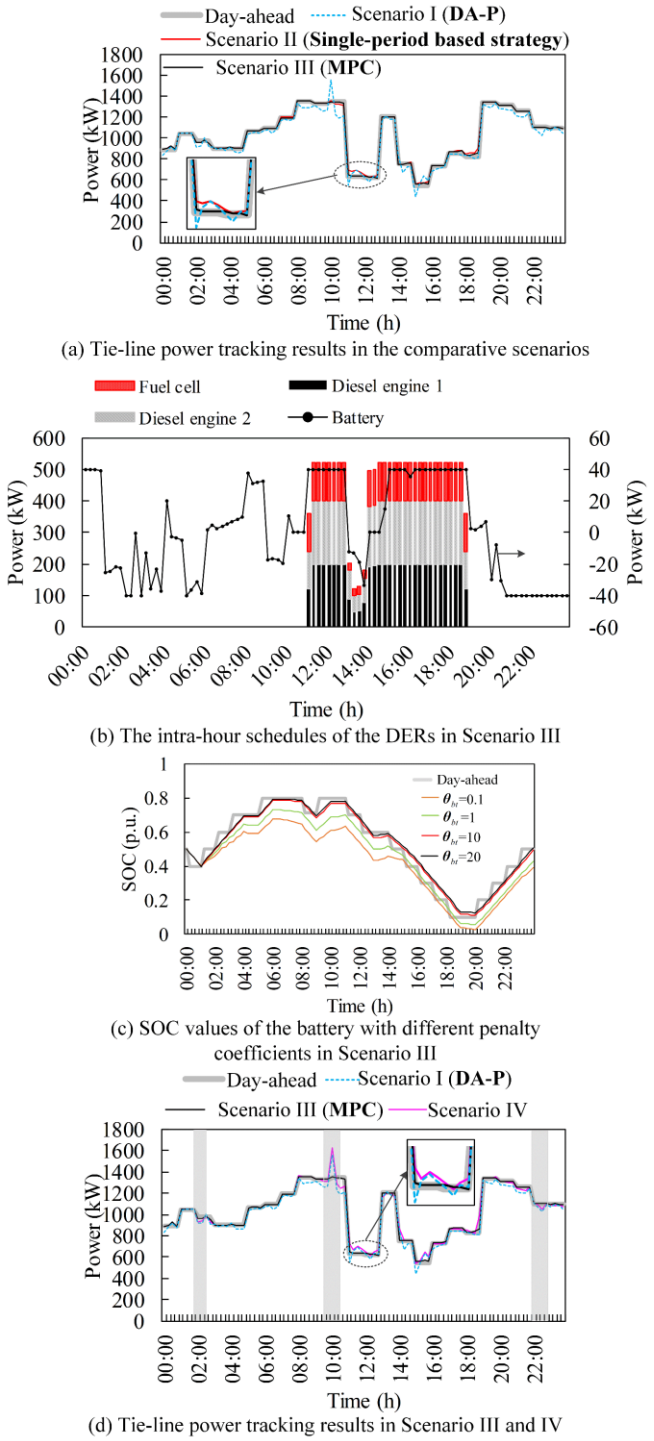


***Fig. 7.*** *Intra-hour rescheduling results under uncertainty level 1*

It can be observed from Fig. 7 (a) that the performance of electric tie-line power tracking in Scenario III is close to that in Scenario II during periods of smooth tie-line power (e.g., 06:00-09:00). However, better performance of tie-line power tracking can be obtained in Scenario III during periods with large tie-line power fluctuations (e.g., 10:00-12:00), as shown in the circled area and enlarged figure in Fig. 7 (a). This observation was attributed to the fact that the MPC based optimisation method used in Scenario III can handle the future behaviour of the BIM over a future time horizon. In this case, the DERs and VESSs can be adjusted in advance to smooth the upcoming large tie-line power fluctuations. In other words, timely adjustments of the DERs and VESSs can be obtained with the MPC based optimisation method in Scenario III. Nevertheless, traditional single-period based optimisation strategy cannot handle the future behaviour of the BIM, the DERs and VESSs are not adjusted in advance accordingly. In this case, the problems of the insufficient adjustments and untimely adjustments of the DERs and VESS occur naturally due to their technical limits. Therefore, it can be concluded that the MPC based optimisation method in Scenario III can improve the control performance for tie-line power tracking.

The intra-hour schedules of the DERs in Scenario III are shown in Fig. 7 (b). The results show that the power outputs of the DGs and battery are adjusted to smooth the fluctuations of tie-line power, while the unit commitment of the DGs and the charging/discharging status of the battery are kept the same with that at day-ahead stage. The SOC values of the battery with different penalty coefficients at intra-hour stage in Scenario III are shown in Fig. 7 (c). The results show that higher value of penalty coefficient leads to better performance of SOC tracking of the battery, and vice versa.

Another comparative scenario is set up further to highlight the effect of VESSs' participation at intra-hour stage as **Scenario IV (MPC based strategy)**. In this scenario, only the DERs are rescheduled using MPC based optimisation strategy, while the VESSs' participations are not considered. The electric tie-line powers in Scenario I, II and IV are shown in Fig. 7 (d). The following conclusions were derived based on the results:

1) The performance of electric tie-line power tracking in Scenario III is better than that in Scenario IV due to VESSs' participation in intra-hour stage;

2) The performance of electric tie-line power tracking in Scenario IV is close to that in Scenario III when the DGs are in 'ON'-state (e.g., 11:00-18:00) due to DGs' participation in intra-hour stage;

3) The performance of electric tie-line power tracking in Scenario IV is as poor as that in Scenario I when the DGs are in 'OFF'-state (e.g., 02:00-03:00, 09:00-10:00 and 22:00-23:00), as shown in the shaded areas in Fig. 7 (d). This is because that the schedulable capacity of the BIM is very limited without DGs and VESSs' participations.

The schedules of VESSs in Scenario III at intra-hour stage are shown in Fig. A8 of Appendix A. Compared to the day-ahead scheduling results of the VESSs in Fig. A7, it can be observed that the schedules of the VESSs (the charging/discharging power of the VESS) are adjusted at the intra-hour stage to smooth the tie-line power fluctuations. Then the cooling schedules of the buildings in Scenario III at intra-hour stage are adjusted accordingly, as shown in Fig. 8. Compared to the day-ahead cooling schedules in Fig. 5, it can be concluded that the indoor temperatures of the buildings and power consumptions of the electric chillers are adjusted considering VESSs' participation at intra-hour stage (as shown in the right side figures in Fig. 8). The intra-hour cooling schedules without VESSs' participation, as shown in the left side figures in Fig. 8, are kept the same with that at day-ahead stage.

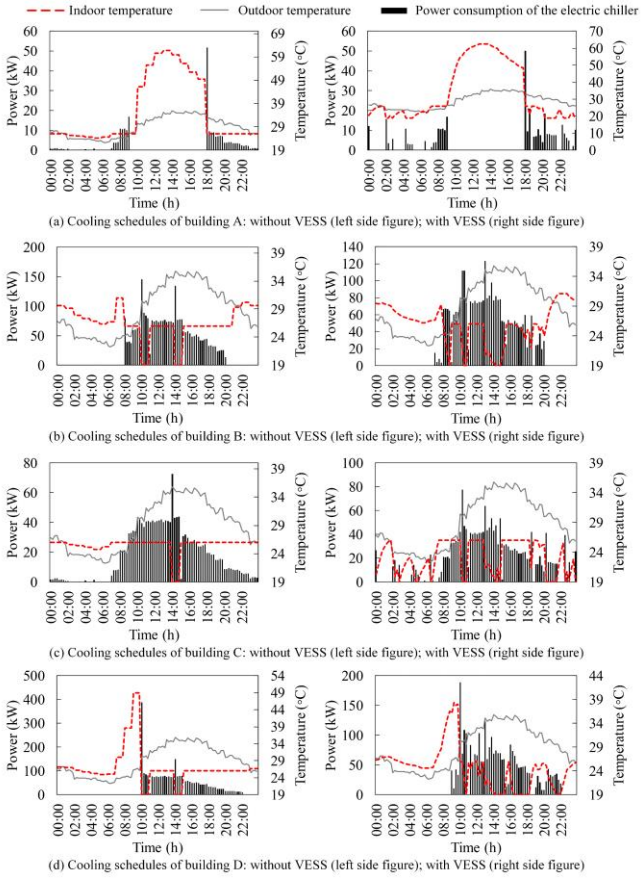


***Fig. 8.*** *Intra-hour cooling schedules of the buildings*

To further validate the effectiveness of the proposed method, the mean square errors (MSEs) of the electric tie-line power under Scenario I - IV are compared, as shown in Eq. (48). The day-ahead set-points of the electric tie-line powers are used as reference values.

$$\begin{cases} MSE_I = \sqrt{\dfrac{1}{t'}\sum_{t'=1}^{n_2}\left(P^{I}_{grid,t'} - P^{dh}_{grid,t'}\right)^2} \\ MSE_{II} = \sqrt{\dfrac{1}{t'}\sum_{t'=1}^{n_2}\left(P^{II}_{grid,t'} - P^{dh}_{grid,t'}\right)^2} \\ MSE_{III} = \sqrt{\dfrac{1}{t'}\sum_{t'=1}^{n_2}\left(P^{III}_{grid,t'} - P^{dh}_{grid,t'}\right)^2} \\ MSE_{IV} = \sqrt{\dfrac{1}{t'}\sum_{t'=1}^{n_2}\left(P^{IV}_{grid,t'} - P^{dh}_{grid,t'}\right)^2} \end{cases} \tag{48}$$

$P^{I}_{grid,t'}$, $P^{II}_{grid,t'}$, $P^{III}_{grid,t'}$ and $P^{IV}_{grid,t'}$ are the electric tie-line powers in the scenarios. The MSEs denote the sample standard deviation between the values under different scenarios and reference values. The smaller value of MSE denotes that the fluctuations of the electric tie-line power is better smoothed. The values of MSE in different scenarios under uncertainty level 1 are shown in Tab. 1, which demonstrate that fluctuations of the electric tie-line power can be well smoothed by scheduling DERs and VESSs using the

proposed MPC based method in Scenario III.

**Table 1** MSEs in different scenarios under uncertainty level 1

| Scenario | MSE |
|---|---|
| I | 12.88 |
| II | 5.02 |
| III | 2.65 |
| IV | 11.73 |

### *4.4. Comparative results under different uncertainty levels of forecasting data*

In order to further verify the effectiveness of the proposed scheduling method, more operational scenarios at intra-hour stage under different uncertainty levels of the forecasting data are carried out in this section. The threshold values of the forecasting errors under different uncertainty levels are shown in Tab. B1. The electric tie-line powers of the BIM with different strategies (i.e., DA-P strategy, Single-period based strategy and MPC based strategy) under uncertainty levels 2 - 3 are shown in Fig. 9 (a) – (b).

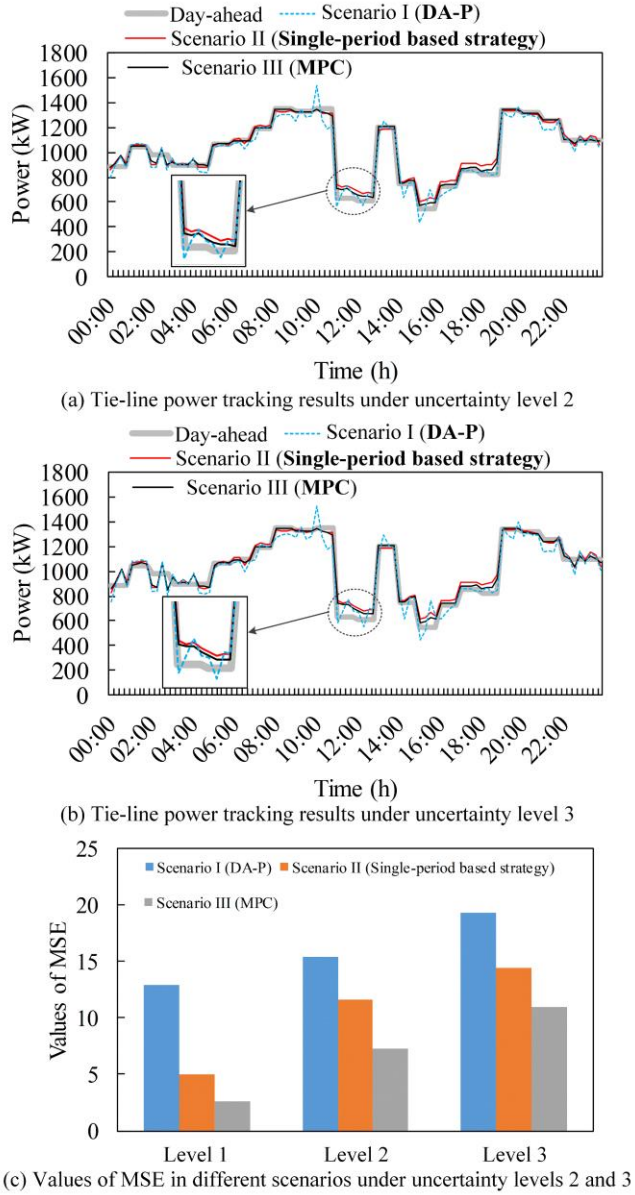


(a) Tie-line power tracking results under uncertainty level 2

(b) Tie-line power tracking results under uncertainty level 3

(c) Values of MSE in different scenarios under uncertainty levels 2 and 3

***Fig. 9.*** *Tie-line powers of the BIM under uncertainty levels 2-3 and their MSE values*

It can be observed from Fig. 9 (a) – (b). that the performance of tie-line power tracking with MPC based strategy is the best under all the uncertainty levels. The values of MSEs of the electric tie-line power in Scenario I - III under uncertainty levels 2 - 3 are further compared in Table 2 and Fig. 9 (c). The results show that the values of MSEs in all the scenarios experience an increase with the increasing of uncertainty levels. However, the values of MSEs in Scenario III using MPC based strategy under all the uncertainty levels are minimum. This further demonstrates the effectiveness and good control performance of the MPC based strategy in a time-varying context with uncertainties associated to forecasting data.

**Table 2** MSEs in different scenarios under uncertainty levels 2 and 3

| Scenario | MSE under uncertainty level 2 | MSE under uncertainty level 3 |
|---|---|---|
| I | 15.38 | 19.35 |
| II | 11.62 | 14.38 |
| III | 7.31 | 11.01 |

### *4.5. Discussions*

It is shown by the case study that the proposed optimal scheduling method is able to reduce the daily operating cost at the day-ahead stage and smooth the fluctuations of the electric tie-line power of the BIM caused by the day-ahead forecasting errors at the intra-hour stage. The DERs and VESSs are scheduled in an optimal way with the proposed method at both stages.

At the day-ahead stage, the optimal schedules of the DERs are mainly determined by the electricity prices and their own technical constraints for operating cost reduction of the BIM. The optimal results of the VESSs are closely related to the occupied hours of the buildings, the thermal parameters of the buildings and the electricity prices. Due to the different occupied hours and different parameters of the buildings, the VESSs are dispatched during different time periods and present different charging/discharging characteristics. Furthermore, the VESS tends to be discharged with higher power during high electricity purchase price periods and be charged with higher power before the discharging process for daily operating cost reduction.

At the intra-hour stage, the rescheduling results of the DERs and the VESSs are mainly related to the mismatches between the energy demand and supply caused by day-ahead forecasting errors, as well as their own technical constraints. It is shown from the comparative analysis under different scenarios that the DERs and VESSs can be adjusted in advance to smooth the upcoming large tie-line power fluctuations with the MPC based strategy. In other words, timely adjustments of the DERs and VESSs can be guaranteed with the MPC based strategy in a time-varying context.

Several benefits can be achieved by considering the VESSs in the optimal scheduling method: 1) The daily operating cost of the BIM is reduced at the day-ahead stage with limited modifications on the Microgrid management system; 2) The total startup and shutdown times of the controllable DGs are decreased at the day-ahead stage; 3) The mismatches between the energy demand and supply can be balanced better at the intra-hour stage.

## 5. Conclusion

This paper proposes a two-stage energy management framework to schedule the DERs and smart buildings of a Microgrid in an optimal way. Optimal schedules are generated for the BIM at the day-ahead scheduling stage to reduce the daily operating cost. In the intra-hour adjustment stage, an MPC based adjustment method is proposed to reschedule the DERs and VESSs to smooth the fluctuations of the electric tie-line power, taking the uncertainties from renewable generation, electric load demand, outdoor temperature and solar radiation into consideration. The following conclusions were derived based on the numerical studies:

(1) The flexibility of the building with its thermal mass can be used effectively by scheduling the VESS in day-ahead stage and rescheduling the VESS in intra-hour stage with the proposed energy management framework.

(2) By using the iterative rolling optimisation with finite horizon (i.e., MPC based optimisation) instead of the traditional open-loop and single-period based optimisation, the problems of the insufficient adjustments and untimely adjustments of the DERs and VESS at intra-hour stage can be solved. The MPC based optimisation method can improve the control performance in a time-varying context with uncertainties associated to forecasting data.

(3) Various practical constraints from the buildings, DERs as well as the electric network of the Microgrid can be considered with the proposed scheduling model and developed co-simulation platform.

There are also limitations for the work carried out, and these are considered as the future research to be undertaken:

(1) The initial set points of the MPC determined by a robust power flow algorithm leads to more robust and efficient control performance against uncertainties for MPC. Therefore, a robust power flow algorithm for the BIM will be investigated to determine the initial set points of the MPC in a more robust and efficient way in our future research work.

(2) The effectiveness of the proposed scheduling method is verified at the algorithm level with comparative cases under different operational scenarios of the BIM. However, experimental test is very important for verification of the proposed scheduling method. Therefore, the experimental platform will be set up for real-time hardware test in our future research work.

(3) We assume the forecasting errors of short-term forecasting data follows the uniform distribution in this study. However, different assumptions of the short-term forecasting errors lead to different rescheduling results at the intra-hour stage. Therefore, the MPC based strategy integrated with forecasting techniques for short-term forecasting data will be studied in our future research work.

## Acknowledgements

This work was supported in part by National Natural Science Foundation of China (Grant No. 51677124, 51625702, 51677022, 51607033, and 51607034), National Key Research and Development Program of China (2017YFB0903300 and 2017YFB0903400), and Integrated Energy System Innovation Team of Jilin Province (20180519015JH), and International Clean Energy Talent Programme (iCET) of China Scholarship Council.

## References

[1] United Nations Department of Economic and Social Affairs Population Division, "World Urbanization Prospects: The 2014 Revision," 2015

[2] 'International Energy Agency, Tracking Clean Energy Progress 2017: Energy Technology Perspectives 2017 Excerpt Informing Energy Sector Transformations', https://www.iea.org/publications/freepublications/publication/TrackingCleanEnergyProgress2017.pdf, accessed 6 June 2017

[3] 'International Energy Agency, World Energy Outlook 2017: A world in transformation', http://www.iea.org/weo2017, accessed 14 November 2017

[4] IPCC. IPCC Fifth Assessment Synthesis Report-Climate Change 2014 Synthesis Report. IPCC Fifth Assess. Synth. Report-Climate Chang. 2014 Synth. Rep. pages: 167.

[5] Huo, T., Ren, H., Zhang, X., et al.: 'China's energy consumption in the building sector: A Statistical Yearbook-Energy Balance Sheet based splitting method', Journal of Cleaner Production, 2018, 185, pp. 665-679

[6] Yao, J., Costanzo, G.T., Zhu, G., et al.: 'Power admission control with predictive thermal management in smart buildings', IEEE Transactions on Industrial Electronics, 2015, 62, (4), pp. 2642-2650

[7] Li, H., Eseye, A., Zhang, J., et al.: 'Optimal energy management for industrial microgrids with high-penetration renewables', Protection and Control of Modern Power Systems, 2017, 2, (1), pp. 12

[8] Zhang, D., Shah, N., Papageorgiou, L G.: 'Efficient energy consumption and operation management in a smart building with microgrid', Energy Conversion and Management, 2013, 74, (74), pp. 209-222

[9] Jin, X., Mu, Y., Jia, H., et al.: 'Dynamic economic dispatch of a hybrid energy microgrid considering building based virtual energy storage system', Applied energy, 2017, 194, pp. 386-398

[10] Zhang, Y., Wang, R., Zhang, T., et al.: 'Model predictive control-based operation management for a residential microgrid with considering forecast uncertainties and demand response strategies', IET Generation, Transmission & Distribution, 2016, 10, (10), pp. 2367-2378

[11] Roy, J. V., Leemput, N., Geth, F., et al.: 'Electric vehicle charging in an office building microgrid with distributed energy resources', IEEE Transactions on sustainable energy, 2014, 5, (4), pp. 1389-1396

[12] Hu, B., Wang, H., Yao, S.: 'Optimal economic operation of isolated community microgrid incorporating temperature controlling devices', Protection and Control of Modern Power Systems, 2017, 2, (1), pp. 6

[13] Wang, Z., Wang, L., Dounis, A. I., et al.: 'Integration of plug-in hybrid electric vehicles into energy and comfort management for smart building'. Energy & Buildings, 2012, 47, (47), pp. 260-266

[14] Shaikh, P.H., Nor, N.B.M., Nallagownden, P., et al.: 'Intelligent multi-objective control and management for smart energy efficient buildings', International Journal of Electrical Power & Energy Systems, 2016, 74, pp. 403-409

[15] Wu, X., Hu, X., Yin, X. et al.: 'Stochastic optimal energy management of smart home with pev energy storage', IEEE Transactions on Smart Grid, 2018, 9, (3), pp. 2065-2075

[16] Thomas, D., Deblecker, O. and Ioakimidis, C.S.: 'Optimal operation of an energy management system for a grid-connected smart building considering photovoltaics' uncertainty and stochastic electric vehicles' driving schedule', Applied Energy, 2018, 210, pp. 1188-1206

[17] Tian, Y., Fan, L., Tang, Y., et al.: 2018. 'A Coordinated Multi-time Scale Robust Scheduling Framework for Isolated power System with ESU under High RES Penetration'. IEEE Access, 2018, 6, pp. 9774 – 9784

[18] Ai, X., Wen, J., Tong, W., et al.: 'A discrete point estimate method for probabilistic load flow based on the measured data of wind power' IEEE Applications Society Meeting, Las Vegas, NV,

USA, Oct. 2012, pp. 2244–2252
[19] Wang, C., Zhou, Y., Wu, J., et al.: 'Robust-index method for household load scheduling considering uncertainties of customer behavior', IEEE Transactions on Smart Grid, 2015, 6, (4), pp. 1806-1818
[20] Wang, C., Zhou, Y., Jiao, B., et al.: 'Robust optimization for load scheduling of a smart home with photovoltaic system', Energy Conversion and Management, 2015, 102, pp. 247-257
[21] Li, Y.Z., Zhao, T.Y., Wang, P., et al.: 'Flexible scheduling of microgrid with uncertainties considering expectation and robustness'. IEEE Transactions on Industry Applications, Niagara Falls, ON, Canada, May 2017, pp. 1–7
[22] Bao, Z., Zhou, Q., Yang, Z., et al.: 'A multi time-scale and multi energy-type coordinated microgrid scheduling solution—Part I: Model and methodology', IEEE Transactions on Power Systems, 2015, 30, (5), pp. 2257-2266
[23] Wang, C., Jiao, B., Guo, L., et al.: 'Robust scheduling of building energy system under uncertainty', Applied energy, 2016, 167, pp. 366-376
[24] Rahmani-Andebili, M.: 'Scheduling deferrable appliances and energy resources of a smart home applying multi-time scale stochastic model predictive control', Sustainable Cities and Society, 2017, 32, pp. 338-347
[25] Jin, X., Wu, J., Mu, Y., et al.: 'Hierarchical microgrid energy management in an office building', Applied Energy, 2017, 208, pp. 480-494
[26] Liu, Y., Wu, F.F.: 'Generator bidding in oligopolistic electricity markets using optimal control: fundamentals and application', IEEE Transactions on Power Systems, 2006, 21, (3), pp. 1050-1061
[27] Martinez, L., Soares, S.: 'Comparison between closed-loop and partial open-loop feedback control policies in long term hydrothermal scheduling', IEEE Transactions on Power Systems, 2002, 17, (2), pp. 330-336
[28] Chen, C., Wang, J., Heo, Y., et al.: 'MPC-Based Appliance Scheduling for Residential Building Energy Management Controller', IEEE Transactions on Smart Grid, 2013, 4, (3), pp. 1401-1410
[29] Guo, Y., Xiong, J., Xu, S., et al.: 'Two-stage economic operation of microgrid-like electric vehicle parking deck', IEEE Transactions on Smart Grid, 2017, 7, (3), pp.1703-1712
[30] Shi W., Li N., Chu C. C., et al.: 'Real-Time Energy Management in Microgrids', IEEE Transactions on Smart Grid, 2017, 8, (1), pp. 228-238
[31] Tanguy K., Dubois M. R., Lopez K. L., et al.: 'Optimization model and economic assessment of collaborative charging using Vehicle-to-Building', Sustainable Cities & Society, 2016, 26, pp.496-506
[32] Rosa, M.D., Bianco, V., Scarpa, F., et al.: 'Heating and cooling building energy demand evaluation; a simplified model and a modified degree days approach', Applied energy, 2014, 128, pp. 217-229
[33] Cristofari, C., Norvaišienė, R., Canaletti, J.L., et al.: 'Innovative alternative solar thermal solutions for housing in conservation-area sites listed as national heritage assets', Energy and Buildings, 2015, 89, pp. 123-131
[34] Yang, I.H., Yeo, M.S., Kim, K.W.: 'Application of artificial neural network to predict the optimal start time for heating system in building. Energy Conversion & Management, 2003, 44, (17), pp. 2791-2809
[35] ISO 13790: 'Energy Performance of Buildings–Calculation of Energy Use for Space Heating and Cooling', 2008
[36] ISO 6946: 'Building Components and Building Elements–Thermal Resistance and Thermal Transmittance–Calculation Method', 2007
[37] Ozel, M., Pihtili, K.: 'Optimum location and distribution of insulation layers on building walls with various orientations', Building & Environment, 2007, 42, (8), pp. 3051-3059
[38] Duffie, J.A., Beckman, W.A. Solar engineering of thermal process. New York: Wiley; 1991.
[39] Zainal, O.A., Yumrutaş, R.: 'Validation of periodic solution for computing CLTD (cooling load temperature difference) values for building walls and flat roofs', Energy, 2015, 82, pp. 758-768
[40] Mayne D. Q., Rawlings J. B., Rao C. V., et al.: 'Constrained model predictive control: Stability and optimality', Automatica, 2000, 36, (6), pp. 789-814
[41] IBM ILOG CPLEX Optimization Solver 12.2
[42] Dugan, Roger C. "Reference guide: The open distribution system simulator (opendss)." Electric Power Research Institute, Inc 7 (2012).
[43] Su, W., Wang, J., Zhang, K., et al.: 'Model predictive control-based power dispatch for distribution system considering plug-in electric vehicle uncertainty', Electric Power Systems Research, 2014, 106, (1), pp. 29-35
[44] Jin, X., Mu, Y., Jia, H., et al.: 'Calculation of Optimal Hybrid Power Flow for Integrated Community Energy System Considering Electric Distribution Network Reconfiguration', Automation of Electric Power Systems, 2017, 41, (1), pp.18-24 and 56
[45] Melo J. L., Teng J. L, Sun S.: 'Online Demand Response Strategies for Non-Deferrable Loads with Renewable Energy', IEEE Transactions on Smart Grid, 2018, 9, (5), pp: 527-5235
[46] Yan, Z., Tao, Z., Liu, Y., et al.: 'Optimal Energy Management of a Residential Local Energy Network Based on Model Predictive Control', Proceedings of the CSEE, 2015, 35, (14), pp. 3656-3666
[47] Wu, X., Wang, X. and Qu, C.: 'A hierarchical framework for generation scheduling of microgrids', IEEE Transactions on Power Delivery, 2014, 29, (6), pp.2448-2457
[48] Li, P., Xu, D., Zhou, Z., et al.: 'Stochastic optimal operation of microgrid based on chaotic binary particle swarm optimization', IEEE Transactions on Smart Grid, 2016, 7, (1), pp. 66-73
[49] Jabbari-Sabet, R., Moghaddas-Tafreshi, S.M. and Mirhoseini, S.S.: 'Microgrid operation and management using probabilistic reconfiguration and unit commitment', International Journal of Electrical Power & Energy Systems, 2016, 75, pp. 328-336
[50] Alharbi, W., Raahemifar, K.: 'Probabilistic coordination of microgrid energy resources operation considering uncertainties', Electric Power Systems Research, 2015, 128, pp. 1-10
[51] Basu, Kumar, A.: 'Microgrids: Planning of fuel energy management by strategic deployment;of CHP-based DERs - An evolu-tionary algorithm approach', International Journal of Electrical Power & Energy Systems, 2013, 44, (1), pp. 326-336

## Appendices

*Appendix A: Figures*

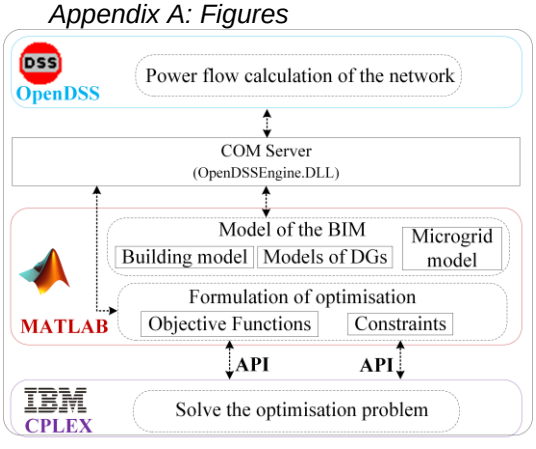


***Fig. A1.*** *Framework of co-simulation*

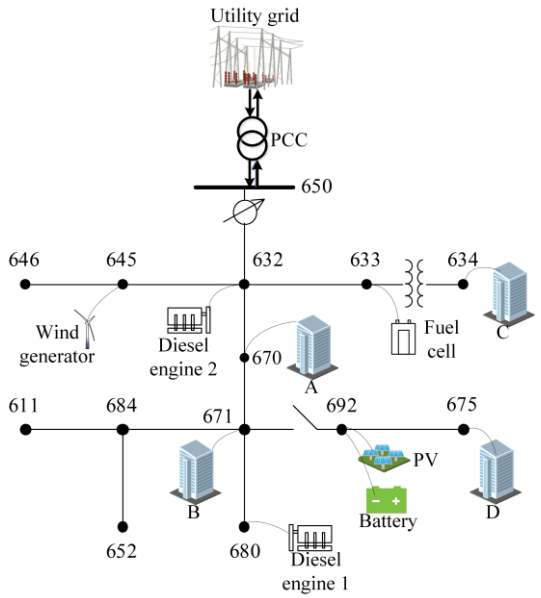


***Fig. A2.*** *A modified IEEE 13 node distribution test feeder*

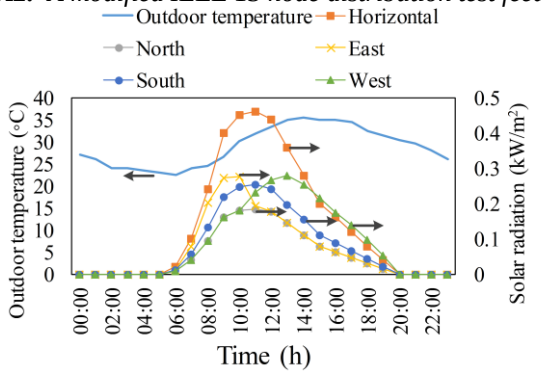


***Fig. A3.*** *Day-ahead forecasting values of the outdoor temperature, solar radiation*

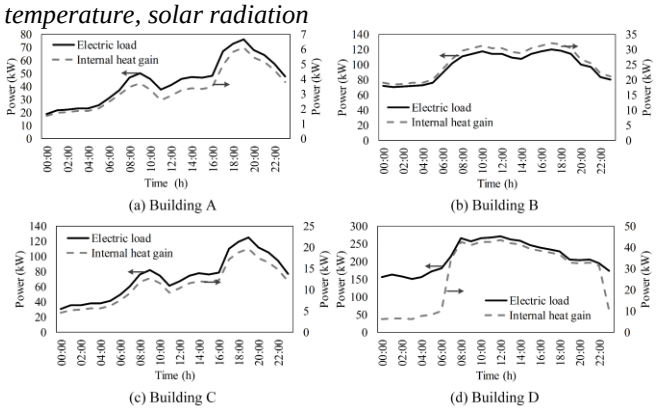


***Fig. A4.*** *Day-ahead forecasting values of the electric loads and internal heat gains of the buildings*

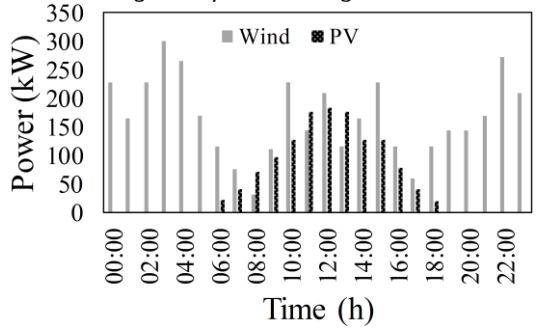


**Table B2** Thermal parameters of the four buildings

***Fig. A5.*** *Day-ahead forecasting values of the renewable generations*

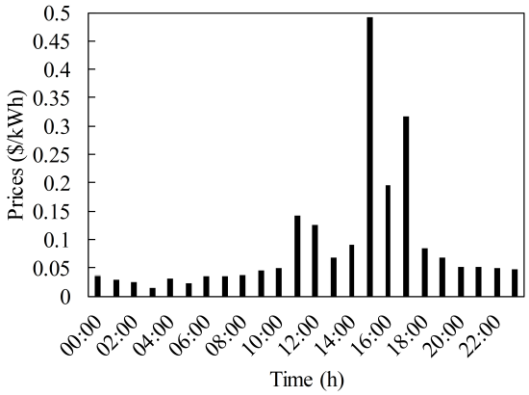


***Fig. A6.*** *Electricity purchasing prices*

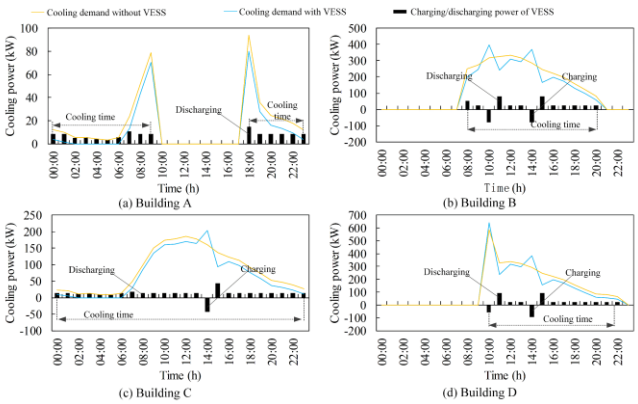


***Fig. A7.*** *Day-ahead schedules of the VESSs*

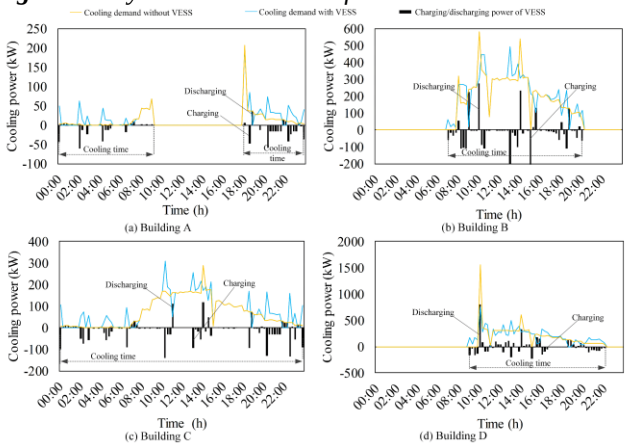


***Fig. A8.*** *Intra-hour schedules of the VESSs*

## *Appendix B: Tables*

**Table B1** Threshold values of the forecasting errors under different uncertainty levels

| | Level 1 | Level 2 | Level 3 |
|---|---|---|---|
| Wind power | 0.20 | 0.40 | 0.6 |
| PV power | 0.12 | 0.24 | 0.36 |
| Load | 0.04 | 0.08 | 0.12 |
| Outdoor temperature | 0.02 | 0.04 | 0.06 |

| No. | $U_{wall}$ [W/(m$^2$·K)] | $F_{wall}$/m$^2$ | $U_{win}$ [W/(m$^2$·K)] | Window to wall ratio (%) | Long side (m) | Short side (m) | Height (m) | Occupied hours |
|---|---|---|---|---|---|---|---|---|
| A | 1.092 | 1000 | 2.800 | 45 | 30 | 20 | 9 | 00:00 -09:00 & 18:00 -23:00 |
| B | 0.908 | 2400 | 2.750 | 75 | 40 | 20 | 30 | 08:00 -20:00 |
| C | 1.146 | 1500 | 2.800 | 60 | 30 | 20 | 20 | Whole day |
| D | 0.820 | 2700 | 2.500 | 65 | 50 | 30 | 20 | 10:00 -22:00 |

**Table B3** Technical parameters of the controllable DGs

| DG type | $\underline{P}_{DG}$ (kW) | $\overline{P}_{DG}$ (kW) | $R_u$ (kW/min) | $R_d$ (kW/min) | $S_u$ (kW/min) | $S_d$ (kW/min) | $UT$ (h) | $DT$ (h) | Number of DG |
|---|---|---|---|---|---|---|---|---|---|
| Diesel engine | 40 | 200 | 8 | 8 | 8 | 8 | 2 | 1 | 2 |
| Fuel cell | 12 | 120 | 8 | 8 | 8 | 8 | 2 | 1 | 1 |

**Table B4** Economic parameters of the DERs

| | Diesel engine | Fuel cell | PV | Wind | Battery | Electric chiller |
|---|---|---|---|---|---|---|
| Startup cost ($) | 0.24 | 0.32 | - | - | - | - |
| Maintenance cost ($) | 0.0033 | 0.0046 | 0.001 | 0.001 | 0.001 | 0.001 |

**Table B5** Parameters of the battery and electric chiller

| **Parameters** | **Value** |
|---|---|
| $COP_{EC}$ | 4 |
| $\overline{P}_{EC,1}$ / $\underline{P}_{EC,1}$ | 120kW/0kW |
| $\overline{P}_{EC,2}$ / $\underline{P}_{EC,2}$ | 200kW/0kW |
| $\overline{P}_{EC,3}$ / $\underline{P}_{EC,3}$ | 120kW/0kW |
| $\overline{P}_{EC,4}$ / $\underline{P}_{EC,4}$ | 600kW/0kW |
| $\overline{P_{ex}}$ / $\underline{P_{ex}}$ | 1350kW/-500kW |
| $CAP_{bt}$ | 400kWh |
| $\overline{SOC}$ / $\underline{SOC}$ | 0.8/0.2 |
| $\overline{P}_{bt}$ / $\underline{P}_{bt}$ | 40kW/-40kW |
| $\eta_{ch}$/$\eta_{dis}$ | 0.95/0.95 |
| $\delta$ | 0.04 |
| $\eta_{FC}$ | 0.55 |